



Global Greenhouse Gas Reconciliation 2022

Zhu Deng^{1,2,3}, Philippe Ciais^{4,*}, Liting Hu⁵, Adrien Martinez⁴, Marielle Saunois⁴, Rona L. Thompson⁶,
Kushal Tibrewal⁴, Wouter Peters^{7,8}, Brendan Byrne⁹, Giacomo Grassi¹⁰, Paul I. Palmer^{11,12}, Ingrid T.
Luijkx⁷, Zhu Liu^{1,2,3,*}, Junjie Liu^{9,13}, Xuekun Fang⁵, Tengjiao Wang¹⁴, Hanqin Tian¹⁵, Katsumasa
5 Tanaka^{4,16}, Ana Bastos¹⁷, Stephen Sitch¹⁸, Benjamin Poulter¹⁹, Clément Alberge²⁰, Aki Tsuruta²¹, Shamil
Maksyutov¹⁶, Rajesh Janardanan¹⁶, Yosuke Niwa^{16,22}, Bo Zheng^{23,24}, Joël Thanwerdas²⁵, Dmitry
Belikov²⁶, Arjo Segers²⁷, Frédéric Chevallier⁴

¹Department of Geography, University of Hong Kong, Hong Kong SAR, China

²Institute for Climate and Carbon Neutrality, University of Hong Kong, Hong Kong SAR, China

10 ³Department of Earth System Science, Tsinghua University, Beijing, China

⁴Laboratoire des Sciences du Climat et de l'Environnement, IPSL, CEA-CNRS-UVSQ, Université Paris-Saclay, Gif-sur-Yvette, France

⁵College of Environmental & Resource Sciences, Zhejiang University, Hangzhou, Zhejiang, China

⁶Norwegian Institute for Air Research (NILU), Kjeller, Norway

15 ⁷Meteorology and Air Quality Department, Wageningen University & Research, Wageningen, the Netherlands

⁸Energy and Sustainability Research Institute Groningen, University of Groningen, Groningen, the Netherlands

⁹Jet Propulsion Laboratory, California Institute of Technology, Pasadena, CA, USA

¹⁰Joint Research Centre, European Commission, Ispra (VA), Italy

¹¹National Centre for Earth Observation, University of Edinburgh, Edinburgh, UK

20 ¹²School of GeoSciences, University of Edinburgh, Edinburgh, UK

¹³Division of Geological and Planetary Sciences, California Institute of Technology, Pasadena, CA, USA

¹⁴Institute of Blue and Green Development, Shandong University, Weihai, China

¹⁵International Center for Climate and Global Change Research, School of Forestry and Wildlife Sciences, Auburn University, Auburn, AL 36849, USA

25 ¹⁶Earth System Division, National Institute for Environmental Studies, Onogawa 16-2, Tsukuba, Ibaraki 305-8506, Japan

¹⁷Department of Biogeochemical Integration, Max Planck Institute for Biogeochemistry, Hans Knöll Str. 10, Jena, Germany

¹⁸Faculty of Environment, Science and Economy, University of Exeter, Exeter, UK

¹⁹NASA Goddard Space Flight Center, Biospheric Sciences Laboratory, Greenbelt, MD 20771, USA

²⁰European Space Agency Climate Office, ECSAT, Harwell Campus, Didcot, Oxfordshire, UK

30 ²¹Finnish Meteorological Institute, P.O. Box 503, 00101, Helsinki, Finland

²²Department of Climate and Geochemistry Research, Meteorological Research Institute (MRI), Nagamine 1-1, Tsukuba, Ibaraki 305-0052, Japan

²³Shenzhen Key Laboratory of Ecological Remediation and Carbon Sequestration, Institute of Environment and Ecology, Tsinghua Shenzhen International Graduate School, Tsinghua University, Shenzhen, 518055, China

35 ²⁴State Environmental Protection Key Laboratory of Sources and Control of Air Pollution Complex, Beijing 100084, China

²⁵Empa, Swiss Federal Laboratories for Materials Science and Technology, Dübendorf, Switzerland

²⁶Center for Environmental Remote Sensing, Chiba University, Chiba, Japan

²⁷TNO, Department of Air quality and Emissions Research, P.O. Box 80015, NL-3508-TA, Utrecht, the Netherland

Correspondence to: Philippe Ciais (philippe.ciais@lsce.ipsl.fr); Zhu Liu (zhuliu@hku.hk)

40 **Abstract.** In this study, we provide an update of the methodology and data used by Deng et al. (2022) to compare the national greenhouse gas inventories (NGHGs) and atmospheric inversion model ensembles contributed by international research teams coordinated by the Global Carbon Project. The comparison framework uses transparent processing of the net ecosystem



exchange fluxes of carbon dioxide (CO₂) from inversions to provide estimates of terrestrial carbon stock changes over managed land that can be used to evaluate NGHGs. For methane (CH₄), and nitrous oxide (N₂O), we separate anthropogenic emissions from natural sources based directly on the inversion results, to make them compatible with NGHGs. Our global harmonized NGHGs database was updated with inventory data until February 2023 by compiling data from periodical UNFCCC inventories by Annex I countries and sporadic and less detailed emissions reports by non-Annex I countries given by National Communications and Biennial Update Reports. For the inversion data, we used an ensemble of 22 global inversions produced for the most recent assessments of the global budgets of CO₂, CH₄ and N₂O coordinated by the Global Carbon Project with ancillary data. The CO₂ inversion ensemble in this study goes through 2021, building on our previous report from 1990 to 2019, and includes three new satellite inversions compared to the previous study, and an improved managed land mask. As a result, although significant differences exist between the CO₂ inversion estimates, both satellite and in-situ inversions over managed lands indicate that Russia and Canada had a larger land carbon sink in recent years than reported in their NGHGs, while the NGHGs reported a significant upward trend of carbon sink in Russia but a downward trend in Canada. For CH₄ and N₂O, the results of the new inversion ensembles are extended to 2020. Rapid increases in anthropogenic CH₄ emissions were observed in developing countries, with varying levels of agreement between NGHGs and inversion results, while developed countries showed a slow declining or stable trend in emissions. Much denser sampling and higher atmospheric CO₂ and CH₄ concentrations by different satellites, are expected in the coming years. The methodology proposed here to compare inversion results with NGHGs can be applied regularly for monitoring the effectiveness of mitigation policy and progress by countries to meet the objective of their pledges. The dataset constructed for this study is publicly available at <https://doi.org/10.5281/zenodo.10841716> (Deng et al., 2024).

1 Introduction

If modeled pathways align with Nationally Determined Contributions (NDCs) declared prior to COP26 (in 2021) until 2030 and do not involve any subsequent increase in ambition, the projected global warming by 2100 would be 2.1-3.4°C (IPCC, 2023). The global stocktake coordinated by the secretariat of the United Nations Framework Convention on Climate Change (UNFCCC) considers data from national greenhouse gas inventories (NGHGs) to assess the collective climate progress to curb emissions. It is expected there will be differences in the quality of NGHGs being reported to the UNFCCC (Perugini et al., 2021). UNFCCC Annex I Parties, which include all OECD (Organisation for Economic Co-operation and Development) countries and several EIT (Economies In Transition) already report annually their emissions following the same IPCC guidelines (IPCC 2006) in a common reporting format, with a time latency of roughly 1.5 years. In contrast, non-Annex I Parties, mostly developing and less developed countries, are currently not required to provide reports as regularly and as detailed as Annex I Parties and in a few cases use different IPCC Guidelines in their National Communications (NC) or Biennial Update Reports (BUR) submitted to the UNFCCC. Non-Annex I Parties are scheduled in 2024 to move to regular



and harmonized reporting of their emissions in the national inventory reports (NIRs) in the format of common reporting tables
75 (CRTs), following the Paris Agreement's enhanced transparency framework (ETF).

The IPCC guidelines for NGHGs encourage countries to use independent information to verify emissions and removals
(IPCC, 1997, 2006, 2019), such as comparisons with independently compiled inventory databases (e.g. IEA, CDIAC, EDGAR,
FAOSTAT), or with atmospheric mole fraction measurements interpreted by atmospheric inversion models (see Section 6.10.2
in IPCC (2019)). Such verification of 'bottom-up' national reports against 'top-down' atmospheric inversion results is not
80 mandatory. However, a few countries (e.g. Switzerland, United Kingdom, New Zealand, and Australia) have already added
inversions as a consistency check of their national reports. In our study, we utilized the latest global inversion results from the
budget assessments of CO₂, CH₄, and N₂O conducted by the Global Carbon Project (GCP), focusing on three ensembles of
inversions with global coverage. Compared to our previous study (Deng et al., 2022), the CO₂ inversion ensemble used in this
study has been updated to the global CO₂ budget of Friedlingstein et al. (2022) that includes nine CO₂ inversions using mole
85 fraction data from the surface network and/or retrieval products from the Greenhouse Gases Observing Satellite (GOSAT) and
Orbiting Carbon Observatory-2 (OCO-2) satellites. The CH₄ inversion ensemble and N₂O inversion (Tian et al., 2023)
ensemble used in this study are also extended to the 2020. As a result, the new ensembles cover up to 2021 for CO₂, 2020 for
CH₄ and 2020 for N₂O, compared to 2019, 2017 and 2016 respectively in our previous study (Deng et al., 2022), allowing us
to track and analyze the most recent flux variations.

90 Our framework to process inversion aims at making them comparable to inventories at countries or groups of countries scale
(ie,with an area larger than the spatial resolution of atmospheric transport models typically used for inversions).
Atmospheric inversions use *a priori* information for the spatial and temporal patterns of fluxes. Some inversions correct prior
fluxes at the spatial resolution of their transport models to match atmospheric observations and use spatial error correlations
(usually e-folding length scales) that tie the adjustment of fluxes from one grid cell to its neighbors at distances of tens to
95 hundreds of kilometers. Other inversions adjust fluxes over coarse regions that are larger than the resolution of the transport
model, implicitly assuming a perfect correlation of flux errors within these regions, causing an aggregation error (Kaminski et
al., 2001). Thus, to minimize aggregation errors, the results of inversions are shown preferentially for selected large area
emitter countries or large absorbers in the case of CO₂. We have selected a different set of countries/groups of countries for
each gas, according to their importance in the global emission budget. According to the median of inversion data we used in
100 this study, selected countries collectively represent ~70% of global fossil fuel CO₂ emissions, ~90% of global land CO₂ sink,
~60% of anthropogenic CH₄ emissions, and ~55% of anthropogenic N₂O emissions. To more robustly interpret global
inversion results for comparison with inventories, we follow the same criterion and choose high-emitting countries covered (if
possible) by atmospheric measurements, although most selected tropical countries have few or no atmospheric in-situ stations.
Uncertainties are given by the spread among inversion models (min-max range given the small number of inversions), and the
105 causes for discrepancies with inventories are analyzed systematically and on a case-by-case basis, considering both individual
countries and specific greenhouse gases, for annual variations and for mean budgets over several years.



Based on the newly updated inversion results and inventory, and an improvement in the methodology framework proposed in the previous study (Deng et al., 2022), we specifically address the following questions: 1) how do inversion models compare with NGHGs for the three gases?; 2) what are the plausible reasons for mismatches between inversions and NGHGs?; and in particular, did the new maps of managed land masks in this study reduce the mismatch between the inversions and NGHGs for CO₂ and N₂O?; 3) what independent information can be extracted from inversions to evaluate the mean values or the trends of greenhouse gas emissions and removals?; and does this information exhibit a good agreement with NGHGs?; and 4) how do satellite-retrieval driven inversion models differ from the surface in-situ and flask sampling driven inversion model results? Sections 2 presents the updated global database of national emissions reports for selected countries and its grouping into sectors, the global atmospheric inversions used for the study, the processing of fluxes from these inversions to make their results as comparable as possible with inventories. The time series of inversions compared with inventories for each gas, with insights on key sectors for CH₄ are discussed in **Sections 3 to 5**. The discussion (Section 6) focuses on the plausible reasons for mismatches between inversions and NGHGs, comparison between inversion ensembles in this study and previous study, and different priors applied in the CH₄ inversions. Finally, concluding remarks are drawn on how inversions could be used systematically to support the evaluation and possible improvement of inventories for the Paris Agreement.

2 Material and methods

2.1 Compilation and harmonization of national inventories reported to the UNFCCC

All UNFCCC Parties shall periodically update and submit their national GHG inventories of emissions by sources and removals by sinks to the Convention parties. Annex I countries submit their NIRs in common reporting format (CRF) tables every year with a complete time series starting in 1990. Non-Annex I Parties are required to submit their NC roughly every four years after entering the Convention and submit BUR, every two years since 2014. Currently, there are in total 427 submissions of NC and over 166 submissions of BUR (UNFCCC, 2021b, a) (**Fig 1**).

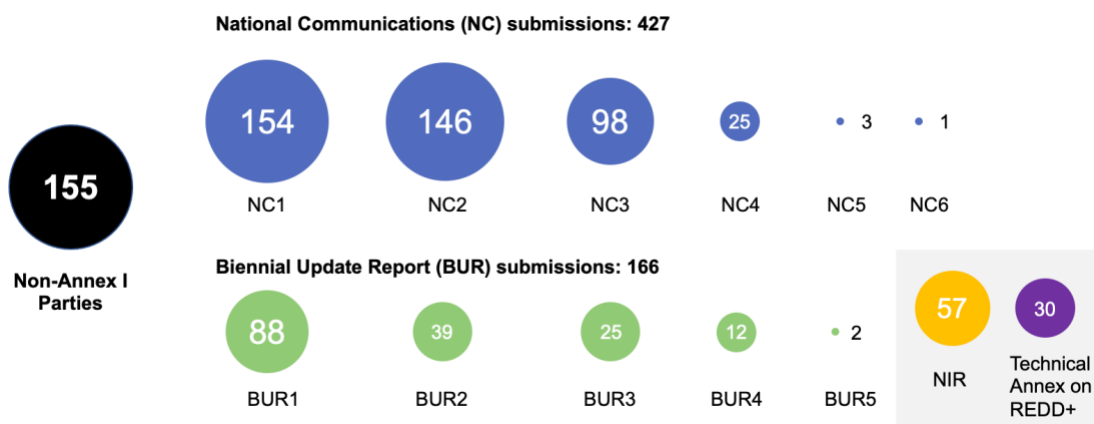




Figure 1. Numbers of non-Annex I parties for each submission round (as of February 28, 2023). The numbers in the middle of the dots
130 denote the numbers of non-Annex I parties for each submission, while the black dots denote the total number of non-Annex I parties, the
blue dots denote the numbers of non-Annex I parties who has submitted National Communications (NC), green dots for Biennial Update
Reports (BUR), yellow dots for National Inventory Report (NIR), and purple dots for Technical Annex on REDD+ . The numbers after the
NC and BUR denote the total number of submission reports.

We collected NGHIGs data submitted to UNFCCC by February 28, 2023. For Annex I countries, data collection is
135 straightforward, as their reports are provided as Excel files under a Common Reporting Format (CRF) until the year 2020 last
accessed on February 28, 2023. For non-Annex I countries, the data were directly extracted from the original reports provided
in Portable Document Format (PDF) last accessed on February 28, 2023. Data from successive reports for the same country
were extracted, except when they relate to the same years, in which case only the latest version is considered. While Annex I
countries are required to compile their inventory following IPCC 2006 guidelines and the subdivision between sectors
140 established by the UNFCCC decision (dec. 24/CP.19), non-Annex I countries are increasingly adopting the IPCC 2006
Guidelines, although some still utilize the older IPCC 1996 Guidelines, with different approaches and sectors. Consequently,
the methods used and the reported sectors may differ among NC and BUR reports.

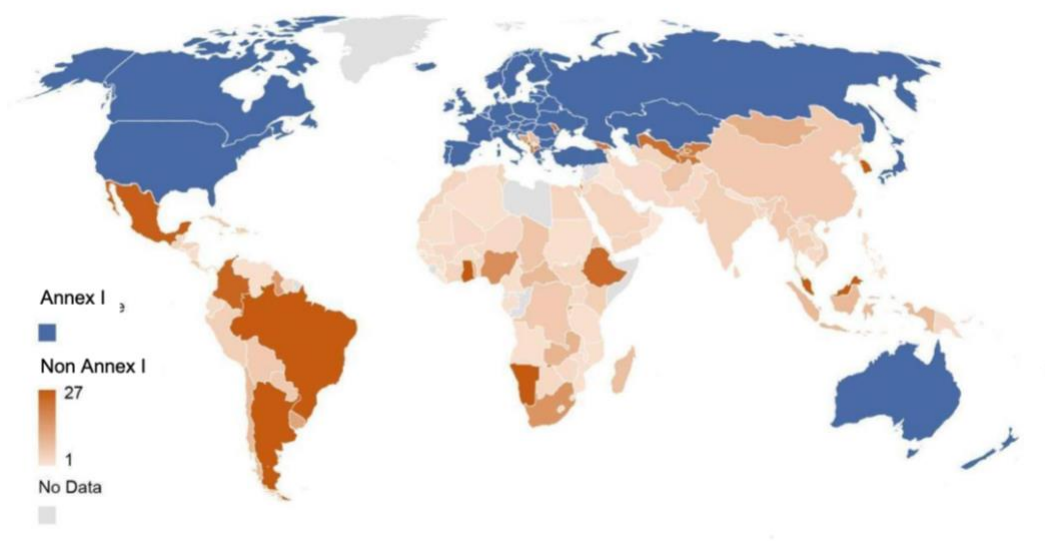


Figure 2. Number of years covered by NGHGI reports (NC+BUR) in each non-Annex I country (as of February 28, 2023). Emissions
145 from Greenland are reported by Denmark.

2.2 Atmospheric inversions

CO₂ inversions

Nine CO₂ inversion systems from the 2022 Global Carbon Budget of the GCP (Friedlingstein et al., 2022) are used, including
CarbonTracker-Europe (CTE) v2022 (van der Laan-Luijkx et al., 2017), Jena CarboSCOPE v2022 (Rödenbeck et al., 2003), the



150 surface air-sample inversion from the Copernicus Atmosphere Monitoring Service (CAMS) v21r1 (Chevallier et al., 2005),
 the inversion from the CAMS Satellite FT21r2 (Chevallier et al., 2005), the inversion from the University of Edinburgh (UoE)
 v6.1b (Feng et al., 2016), the NICAM-based Inverse Simulation for Monitoring CO₂ (NISMON-CO₂) v2022.1 (Niwa et al.,
 2022), CMS-Flux v2022 (Liu et al., 2021), GONGGA v2022 (Jin et al., 2023), and THU v2022 (Kong et al., 2022). A variety
 of transport models are used by these systems, which allows for representing a major driver factor behind differences in flux
 155 estimates based on atmospheric inversions, particularly their distribution over latitudinal bands. Among the nine inversions,
 four systems (CAMS Satellite FT21r2, GONGGA v2022, THU v2022, and CMS-Flux v2022) utilize satellite CO₂ column
 retrievals from GOSAT and/or OCO-2, calibrated to the World Meteorological Organization (WMO) 2019 standards. CMS-
 Flux additionally incorporates in-situ observed CO₂ mole fraction records. The remaining five inversion systems (CAMS
 v21r1, CTE v2022, Jena Carboscope v2022, UoE v6.1b, and NISMON-CO₂ v2022.1) solely rely on CO₂ mole fractions that
 160 were observed in-situ or collected in flasks (Schuldt et al., 2021, 2022). The CO₂ inversion records extend up to and including
 2021. Their flux estimates are available at https://meta.icos-cp.eu/objects/GahdRITjT22GGmq_GCi4o_wy and details are
 summarized in **Table 1**.

Table 1 | Atmospheric CO₂ inversions used in this study (Friedlingstein et al., 2022)

Inversion System	Version	Period	Observation
CarbonTracker Europe (CTE): CTE2022_SiB4 (van der Laan-Luijkx et al., 2017)	v2022	2001-2021	
Jena Carboscope sEXTocNEET (Rödenbeck et al., 2003)	v2022	1960-2021	
Copernicus Atmosphere Monitoring Service (CAMS) (Chevallier et al., 2005)	v21r1	1979-2021	Ground-based Obspack GLOBALVIEW plus v7.0 and NRT_v7.2
The University of Edinburgh (UoE) (Feng et al., 2016)	v6.1b	2001-2021	
the NICAM-based Inverse Simulation for Monitoring CO ₂ (NISMON-CO ₂) (Niwa et al., 2022)	v2022.1	1990-2021	
CMS-Flux (Liu et al., 2021),	v2022	2010-2021	Ground-based & ACOS-GOSAT v9r; OCO-2 v10 scaled to WMO2019
CAMS-Satellite (Chevallier et al., 2005)	FT21r2	2010-2021	bias-corrected ACOS GOSAT v9 over land until August 2014 + bias- corrected ACO S OCO-2 v10 over land, both rescaled to WMO2019
THU (Kong et al., 2022)	v2022	2015-2021	OCO-2 v10r data scaled to WMO2019
GONGGA (Jin et al., 2023)	v2022	2015-2021	OCO-2 v10r data scaled to WMO2019



CH₄ inversions

165 The CH₄ emissions come from the new ensemble of inversions (Saunois et al. in prep.) from 2000 to 2020, using seven different
 inverse systems for a total nine inversions (**Table 2**). The inverse systems include: CarbonTracker-Europe CH₄ (Tsuruta et
 al., 2017), LMDZ-PYVAR (Yin et al., 2015; Zheng et al., 2018), CIF-LMDZ(Berchet et al., 2021), MIROC4-ACTM (Patra
 et al., 2018; Chandra et al., 2021), NISMON-CH₄ (Niwa et al., 2022), NIES-TM-FLEXPART (Wang et al., 2019; Maksyutov
 et al., 2021), and TM5-CAMS (Segers and Houweling, 2017). This ensemble of inversions gathers various chemistry transport
 170 models, differing in vertical and horizontal resolutions, meteorological forcing, advection and convection schemes, and
 boundary layer mixing. Including these different systems is a conservative approach that allows to cover different potential
 uncertainties of the inversion, among them: model transport, set-up issues, and prior dependency. All inversions except two,
 use updated common prior emission maps for natural and anthropogenic prior emissions divided into 12 sectors, particularly
 the EDGAR v6 inventory for prior fossil fuel emissions (Crippa et al., 2021a extrapolated to Jan 1st, 2021), GFED for fires
 175 and ecosystem models for wetland emissions. During the production of the inversion simulations, it was proposed to use
 another prior for fossil fuel sources, GAINS inventory (REF) instead of . GAINS has higher fossil emissions, in particular over
 the US and a higher increase of fossil emissions over time in the US (Tibrewal et al., 2024). As Tibrewal et al. showed that
 inversions are strongly attracted to their priors, comparison between results with GAINS and EDGAR v6 priors is informative
 about how robust are inversions to their priors when they are used to ‘verify’ NGHGs.

180 Some inversions optimize emissions in groups of sectors, and others only provide total gridded emissions. For the latter, we
 computed the emission from each sector within each pixel based on the proportion of the prior fluxes. The inversions
 assimilating surface stations mole fraction observations provide results since 2000, and those assimilating satellite observations
 from column CH₄ measurements (XCH₄) of the GOSAT satellite provide results since 2010, first full year of
 GOSAT observations. Inversion results were gridded into 1° by 1° monthly emission maps and aggregated nationally using a
 185 country mask (Klein Goldewijk et al., 2017).

Table 2 | Atmospheric CH₄ inversions used in this study (Saunois et al. in prep.)

Inversion system	Abbreviation	Institution	Observations	Period
Carbon Tracker-Europe CH ₄	CTE	FMI	Surface stations	2000-2020
CIF-LMDz	CIF-LMDz	LSCE/CEA	Surface stations	2000-2020
LMDz-PYVAR	PYVAR-LMDz	LSCE/CEA	GOSAT Leicester v7.2	2010-2020
MIROC4-ACTM	MIROC4-ACTM	JAMSTEC	Surface stations	2000-2020
NISMON-CH ₄	NISMON-CH ₄	NIES/MRI	Surface stations	2000-2020
NIES-TM-FLEXPART (NTF)	NIES	NIES	Surface stations	2000-2020
NIES-TM-FLEXPART (NTF)	NIES	NIES	Surface + GOSAT NIES L2 v02.95	2010-2020



TM5-CAMS	TM5	TNO/VU	Surface stations	2000-2020
TM5-CAMS	TM5	TNO/VU	GOSAT ESA/CCI v2.3.8 (combined with surface observations)	2010-2020

N₂O inversions

Four N₂O inversion systems from the updated GCP Nitrous Oxide Budget (Tian et al., 2023) are used: INVICAT (Wilson et al., 2014), PyVAR-CAMS (Thompson et al., 2014), MIROC4-ACTM (Patra et al., 2018, 2022) and GEOS-Chem (Wells et al., 2015). The N₂O inversion results are updated up to 2020.

Table 3 | Atmospheric N₂O inversions used in this study (Tian et al., 2023)

Inversion system	Institution	Period
INVICAT (Wilson et al., 2014)	Univ. Leeds	1995-2020
PyVAR-CAMS (Thompson et al., 2014),	NILU/LSCE	1995-2020
MIROC4-ACTM (Patra et al., 2018, 2022)	JAMSTEC	1997-2019
GEOS-Chem (Wells et al., 2015)	Univ. Minnesota	1995-2019

Aggregating the gridded inversion results into national totals

To obtain national annual-scale flux estimates, we aggregated the gridded flux maps of each inversion with various native resolutions following the methodology outlined in Chevallier (2021). This involved using the 0.08° x 0.08° land country mask of Klein Goldewijk et al. (2017) to calculate the fraction of each country in each inversion grid box.

2.3 Processing of CO₂ inversion data for comparison with NGHGs

Fossil fuel emissions re-gridding - managed land mask

To analyze terrestrial CO₂ fluxes, we subtracted the same fossil fuel emissions (including cement) of GridFEDv2022.2 (Jones et al., 2022) from the total CO₂ flux of each inversion. This is equivalent to assuming perfect knowledge of fossil emissions, adding up to a global total of 9.7 GtC/yr for the year 2021. The dataset used national annual emissions estimates from the 2022 global carbon budget (Friedlingstein et al., 2022) which uses the reported NGHGs data from Annex I countries and are assumed to be broadly consistent with the non-Annex I countries. This assumption may lead to underestimating the uncertainty of terrestrial CO₂ fluxes deduced from inversions.

As defined in the IPCC Guidelines for NGHGs (IPCC, 2006), only CO₂ emissions and removals from managed land are reported in NGHGs as a proxy for human-induced effects (direct effects and indirect effects such as CO₂ fertilization and nitrogen deposition). However, inversion models retrieve all CO₂ fluxes (due to both direct and indirect effects, plus the natural



interannual variability) over all lands. We thus retained inversions' national estimates of the Net Ecosystem Exchange (NEE) CO₂ flux ($F_{ML}^{inv\ NEE}$) over managed lands grid cells only (ML , here defined as all land except intact forests) because the fluxes over unmanaged land are not counted by NGHGs. We use NEE from the definition of Ciais et al. (2020), representing all non-fossil CO₂ exchange fluxes between terrestrial surfaces and the atmosphere. Other work may use Net Biome Production (NBP) with a similar meaning. CO₂ fluxes over unmanaged lands were excluded from the terrestrial CO₂ flux totals that will be compared with NGHGs, proportional to their presence in each inversion grid box. The new maps of non-intact forests are compiled by Grassi et al. (2023). These maps include official country-managed forest and other managed land areas for Canada and Brazil used for their NGHGs, and the intact forest map (Potapov et al., 2017) as a substitute for unmanaged land where country-based information is not available. For Russia, we used non-intact forest maps for each province with thresholds adjusted to match the official managed land areas from Russia's NIRs, and assumed that all grasslands were managed. This approach assumes that non-intact forest areas can serve as a reasonably good proxy for managed forests reported in the NGHGs (Grassi et al., 2021, 2023). It is important to note that this approach is somewhat arbitrary, as highlighted in previous studies (Ogle et al., 2018; Chevallier, 2021; Grassi et al., 2021). However, in the absence of a machine-readable definition of managed plots in many NGHGs, there is currently no better alternative available.

Adjusting CO₂ fluxes due to lateral carbon transport by crop and wood products trade and by rivers

In addition to the extraction of managed land CO₂ flux, there are CO₂ fluxes that are part of $F_{ML}^{inv\ NEE}$ but are not counted by NGHGs. These fluxes are induced by (i) soils to rivers to oceans carbon export (F_{ML}^{rivers}) which has an anthropogenic and a natural component (Regnier et al., 2013), and (ii) net anthropogenic export of crop and wood products across each country's boundary ($F_{ant}^{crop\ trade}$ and $F_{ant}^{wood\ trade}$). The magnitudes of these CO₂ fluxes are different between countries, and values from the selected countries are presented in **SI Fig 1**. We assume that NGHGs include CO₂ losses from fire (wildfire and prescribed fire) and other disturbances (wind, pests) and from domestic harvesting, as recommended by the IPCC reporting guidelines (IPCC, 2006, 2019) (although some countries, such as Canada and Australia exclude some emissions from these disturbances, and the subsequent removals from the same areas (Grassi et al., 2023)). The adjusted inversion NEE that can be compared with inventories, $F_{adj}^{inv\ NEE}$, is given by:

$$F_{adj}^{inv\ NEE} = F_{ML}^{inv\ NEE} - F_{ML}^{rivers} - F_{ant}^{crop\ trade} - F_{ant}^{wood\ trade} \Leftrightarrow F_{ant}^{ni}, \quad (1)$$

where the sign \Leftrightarrow means 'compared with', F_{ant}^{ni} is the anthropogenic CO₂ flux from NGHGs, F_{tot}^{rivers} is the sum of the natural and anthropogenic CO₂ flux on land from CO₂ fixation by plants that is leached as carbon via soils and channeled to inland waters to be exported to the ocean or to another country. All countries export river carbon, but some countries also receive river inputs, e.g., Romania receives carbon from Serbia via the Danube River. We estimated the lateral carbon export by rivers minus the imports from rivers entering each country, including dissolved organic carbon, particulate organic carbon and dissolved inorganic carbon of atmospheric origin distinguished from lithogenic, by using the data and methodology described by Ciais et al. (2021). Data are from Mayorga et al. (2010) and Hartmann et al. (2009) and follow the approach of Ciais et al.



(2021) proposed for large regions. We also extracted the lateral flux by rivers over the managed land by using the same
240 methodology as inversion CO₂ flux. Thus, in a country that only exports river carbon to the ocean, the amount of carbon
exported is equivalent to an atmospheric CO₂ sink, denoted as F_{ML}^{rivers} as in eq. (1), thus ignoring burial, which is a small term.
Over a country that receives carbon from rivers flowing into its territory, a small national CO₂ outgassing is produced by a
fraction of this imported flux. In that case, we assumed that the fraction of outgassed to incoming river carbon is equal to the
fraction of outgassed to soil-leached carbon in the RECCAP2 region to which a country belongs, estimated with data from
245 Ciais et al. (2021).

$F_{ant}^{crop\ trade}$ is the sum of CO₂ sinks and sources induced by the trade of crop products. This flux was estimated from the annual
trade balance of crop commodities calculated for each country from data from the United Nations Statistics Division of the
Food and Agriculture Organization (FAOSTAT) combined with the carbon content values of each commodity (Xu et al.,
2021). All the traded carbon in crop commodities is assumed to be oxidized as CO₂ in one year, neglecting stock changes of
250 products, and the fraction of carbon from crop products going to waste pools and sewage waters after consumption, thus not
necessarily oxidized to atmospheric CO₂. $F_{ant}^{wood\ trade}$ is the sum of CO₂ sinks and sources induced by the trade of wood
products (Zscheischler et al., 2017). Here, we followed Ciais et al. (2021) who used a bookkeeping model to calculate the
fraction of domestically produced and imported carbon in wood products that are oxidized in each country during subsequent
years, with product lifetimes defined by Mason Earles et al (2012). The underlying assumption in estimating CO₂ fluxes from
255 wood harvest is that the emissions from domestically harvested wood, in addition to imported wood minus exported wood that
is not allocated to wood product pools, are released into the atmosphere during the year of harvest. Conversely, wood allocated
to wood product pools is gradually released into the atmosphere over time, based on their respective lifetimes. Domestic
harvest is assumed to be balanced by an atmospheric CO₂ sink of equivalent magnitude, which is not necessarily the case given
that harvest is rarely in equilibrium with forest increment, but inversions NEE will correct for this imbalance in our results,
260 and can thus be compared with NGHGs. We included in the $F_{ant}^{crop\ trade}$ flux the emissions of CO₂ by domestic animals
consuming specific crop products delivered as feed. On the other hand, emissions of CO₂ from grazing animals and the
decomposition of their manure are supposed to occur in the same grid box where grass is grazed, so that the CO₂ net flux
captured by an inversion is comparable with grazed grasslands' carbon stock changes of inventories. Emissions of reduced
carbon compounds (VOCs, CH₄, CO) are not included in this analysis (see Ciais et al. (2021) for a discussion of their
265 importance in inversion CO₂ budgets).

In summary, the purpose of the adjustment of eq. (1) is to make inversion output comparable to the NGHGs that do not include
 F_{ML}^{rivers} , $F_{ant}^{crop\ trade}$ and $F_{ant}^{wood\ trade}$. The UNFCCC accounting rules (IPCC, 2006) assume that all the harvested wood
products are emitted in the territory of a country that produces them, which is equivalent to ignoring $F_{ant}^{wood\ trade}$ as a national
sink or source of CO₂, hence the need to remove $F_{ant}^{wood\ trade}$ from inversion NEE. The adjusted inversion fluxes from eq. (1)
270 depict the national CO₂ stock change which match better the carbon accounting system boundaries of UNFCCC NGHGs. In
the following, we will only discuss adjusted inversion CO₂ fluxes ($F_{adj}^{inv\ NEE}$), but for simplicity call them “inversion fluxes”.



2.4 Processing of CH₄ inversions for comparison with national inventories

Most atmospheric inversions derive total net CH₄ emissions at the surface as it is difficult for them to disentangle overlapping emissions from different sectors at the pixel/regional scale based on atmospheric CH₄ observations only. However, six of the
275 seven inverse systems solve for some source categories owing to different spatio-temporal distributions between the sectors. For each inversion, monthly gridded posterior flux estimates were provided at 1°x1° grid resolution for the net flux at the surface (E_{net}^{inv}), the soil uptake at the surface (E_{soil}^{inv}), the total emission at the surface (E_{tot}^{inv}) and five emitting ‘super sectors’ which regroup several IPCC sectors: Agriculture & Waste (E_{AgW}^{inv}), Fossil Fuel (E_{FF}^{inv}), Biomass & Biofuel Burning (E_{BB}^{inv}), Wetlands (E_{Wet}^{inv}), and Other Natural (E_{Oth}^{inv}) emissions. Considering the soil uptake as a ‘negative source’ given separately, the
280 following equations apply:

$$E_{net}^{inv} = E_{tot}^{inv} + E_{soil}^{inv} = E_{AgW}^{inv} + E_{FF}^{inv} + E_{BB}^{inv} + E_{Wet}^{inv} + E_{Oth}^{inv} + E_{soil}^{inv} \quad (2)$$

For inversions solving for net emissions only, the partition to source sectors was created based on using a fixed ratio of sources calculated from prior flux information at the pixel scale. For inversions solving for some categories, a similar approach was used to partition the solved categories to the five aforementioned emitting sectors. Such processing can lead to significant
285 uncertainties if not all sources increase or change at the same rate in a given region/pixel. National values have been estimated using the country land mask described in the CO₂ section, thus offshore emissions are not counted as part of inversion results unless they are in a coastal grid cell.

In our previous study (Deng et al., 2022), four methods were proposed to separate CH₄ anthropogenic emissions from inversions (E_{Anth}^{inv}) to compare them with national inventories (E_{Anth}^{ni}). The calculations of anthropogenic emissions by each
290 method were performed separately for GOSAT inversions and in-situ inversions. However, the differences in the calculated results among the four methods were smaller compared to the variations observed in the inversions (see Deng et al. (2022) Fig 9). Therefore, we apply only one method in this study which consists of using inversion partitioning as defined in Saunio et al. (2020):

$$E_{Anth}^{inv} = E_{AgW}^{inv} + E_{FF}^{inv} + E_{BB}^{inv} - E_{wildfires}^{BU} \Leftrightarrow E_{Anth}^{ni} \quad (3)$$

This method has some uncertainties. First, the partitioning relies on prior fractions within each pixel, and second, emissions from wildfires are counted for in the Biomass and Biofuel burning (BB) inversion category while they are not necessarily reported in NGHGs. The BB inversion category includes methane emissions from wildfires in forests, savannahs, grasslands, peats, agricultural residues, and the burning of biofuels in the residential sector (stoves, boilers, fireplaces). Therefore, we subtracted bottom-up (BU) emissions from wildfires ($E_{wildfires}^{BU}$) based on the GFEDv4 dataset (van Wees et al., 2022) using
300 their reported dry matter burned and CH₄ emission factors. Because the GFEDv4 dataset also reports specific agricultural and waste fire emissions data, we assumed that those fires (on managed lands) are reported by NGHGs, so they were not counted in $E_{wildfires}^{BU}$.



2.5 Processing of N₂O inversions for comparison with inventories

We subtracted estimates of natural N₂O sources from the N₂O emission budget (E_{tot}^{inv}) of each inversion, to provide inversions
305 of anthropogenic emissions (E_{ant}^{inv}) that can be compared with national inventories (E_{ant}^{ni}).

$$E_{ant}^{inv} = E_{ML}^{inv} - E_{nat}^{aq} - E_{wildfires}^{GFED} \Leftrightarrow E_{ant}^{ni} \quad (4)$$

In our previous study, intact forest grid cells (assumed unmanaged) from Potapov et al. (2017) and lightly grazed grassland
areas from Chang et al. (2021) were removed from the gridded N₂O emissions in proportion to their presence in each inversion
grid box. Here we used the new managed land mask defined in **Section 2.3** to filter gridded N₂O emissions from inversions
310 We verified that the inversion grid box fractions classified as unmanaged do not contain point source emissions from the
industry, energy, and diffuse emissions from the waste sector, to make sure that we do not inadvertently remove anthropogenic
sources by masking unmanaged pixels. From the EDGARv4.3.2 inventory (Janssens-Maenhout et al., 2019), we found that
N₂O from wastewater handling covers a relatively large area that might be partly located in unmanaged land. But the
corresponding emission rates are more than 1 order of magnitude smaller than those from agricultural soils. For other sectors,
315 only very few of the unmanaged grid boxes contain point sources, and none of them have an emission rate that is comparable
with agricultural soils (managed land). Thus, our assumption that emissions from these other anthropogenic sectors are
primarily over managed land pixels is solid (other sectors include: the power industry; oil refineries and transformation
industry; combustion for manufacturing; aviation; road transportation no resuspension; railways, pipelines, off-road transport;
shipping; energy for buildings; chemical processes; solvents and products use; solid waste incineration; wastewater handling;
320 solid waste landfills).

The flux E_{nat}^{aq} is the natural emission from freshwater systems given by a gridded simulation of the DLEM model (Yao et al.,
2019) describing pre-industrial N₂O emissions from N leached by soils and lost to the atmosphere by rivers in the absence of
anthropogenic perturbations (considered as the average of 1900-1910). Natural emissions from lakes were estimated only at a
global scale by Tian et al. (2020), and represent a small fraction of rivers' emissions. Therefore, they are neglected in this
325 study. The flux $E_{wildfires}^{GFED}$ is based on the GFED4s dataset (van Wees et al., 2022) using their reported dry matter burned and
N₂O emission factors. Because the GFED dataset reports specific agricultural and waste fire emissions data, we assume that
those fires (on managed lands) are reported by NGHGs so they were not counted in $E_{wildfires}^{GFED}$ just like for CH₄ emissions.
Note that there could also be a background natural N₂O emission from natural soils over managed lands ($E_{managed\ land}^{soil}$) which
is not necessarily reported by NGHGs. We did not try to subtract this flux from managed land emissions because we assumed
330 that, after a land use change from natural to fertilized agricultural land, background emissions decrease and become very small
compared to N-fertilizers induced anthropogenic emissions. In a future study, we could use for $E_{managed\ land}^{soil}$ the estimate
given by simulations of pre-industrial N₂O emissions from the NMIP ensemble of dynamic vegetation models with carbon-
nitrogen interactions (number of models; n = 7). Namely, their simulation S0 in which climate forcing is recycled from 1901-
1920; CO₂ is at the level of 1860, and no anthropogenic nitrogen is added to terrestrial ecosystems (Tian et al., 2019).



335 Another important point to ensure a rigorous comparison between inversion and NGHGI data is whether anthropogenic indirect
emissions (AIE) of N₂O are reported in NGHGI reports. This is not always the case even though UNFCCC parties are required
to report these in their NGHGIs according to the IPCC guidelines. For example, South Africa's BUR3 did not report indirect
N₂O emissions due to the lack of activity data. AIE arise from anthropogenic nitrogen from fertilizers leached to rivers and
anthropogenic nitrogen deposited from the atmosphere to soils. AIEs represent typically 20% of direct anthropogenic emissions
340 and cannot be ignored in a comparison with inversions. For Annex I countries, AIEs are systematically reported, generally
based on emission factors since these fluxes cannot be directly measured, and we assumed that indirect emissions only occur
on managed land. For non-Annex I countries, we checked manually from the original NC and BUR documents if AIE was
reported or not by each non-Annex I country. If AIEs were reported by a country, they were used as such to compare NGHGI
data with inversion results, and grouped into the agricultural sector. If they were not reported, or if their values were outside
345 plausible ranges, AIE were independently estimated by the perturbation simulation of N fertilizers leaching, CO₂ and climate
on rivers and lakes fluxes in the DLEM model (Yao et al., 2019), and by the perturbation simulation of atmospheric nitrogen
deposition on N₂O fluxes from the NMIP model ensemble (Tian et al., 2019).

2.6 Grouping sectors for comparison

The bottom-up NGHGIs are compiled based on activity data (statistics) following the IPCC 1996/2006 Guidelines (IPCC,
350 1997, 2006) with detailed information on subsectors. However, the top-down inversions can only distinguish between very
few groups of sectors at most. Thus, in this study, we aggregated NGHGI sectors into some 'super sectors' to make inversions
and inventories comparable for each GHG (**Table 2**). For CO₂, the inversions are divided into two aggregated super-sectors:
fossil fuel and cement CO₂ emissions, and adjusted net land flux. Inversions use a prior gridded fossil fuel dataset as
summarized in **Section 1.2**, thus, in this study, we compare only the net land flux between inversions and inventories. To
355 calculate the net land flux over managed lands from NGHGIs, we subtracted fossil emissions from the IPCC/CRF *1. Energy*
and *2. Industrial Processes* (or *2. Industrial Processes and Product Use*) sectors from the *Total GHG emissions including*
LULUCF/LUCF (or *Total national emissions and removals*) sector. For CH₄, we compare inversions and inventories based on
three super sectors, including *Fossil*, *Agriculture and Waste*, and *Total Anthropogenic*. To compare with NGHGIs, we group
the IPCC/CRF sectors of *1. Energy* and *2. Industrial Processes* (or *2. Industrial Processes and Product Use*) by excluding
360 Biofuel Burning (reported under *1. Energy* sector) into the super sector of *Fossil*; we group sectors of *4. Agriculture* (or *3.*
Agriculture) and *6. Waste* (or *5. Waste*) into the super sector of *Agriculture and Waste*; and we aggregate anthropogenic flux
from *Fossil* and *Agriculture and Waste* and *Biofuel Burning* into *Anthropogenic*. For N₂O, we grouped the NGHGI sectors
into *Anthropogenic* flux being the sum of *1. Energy* + *2. Industrial Processes* (or *2. Industrial Processes and Product Use*) +
4. Agriculture (or *3. Agriculture*) + *6. Waste* (or *5. Waste*) + *Anthropogenic Indirect Emissions*.

365 **Table 2. Grouping of NGHGIs sectors into aggregated 'super-sectors' for comparisons with inversions.** * Biofuel burning is likely not
included in NGHGIs but under *1.A.4 Other Sectors* if it is reported. ** Field burning of agricultural residues is reported in Annex I countries



under the Agricultural sector. Note that indirect N₂O emissions are reported by Annex I countries but not systematically by non-Annex I ones

Gas	Super-Sectors	Inversions	NGHGs (IPCC/CRF)
CO ₂	<i>Net Land (adjusted)</i>	<i>Flux Total - Fossil - lateral C</i>	Non-Annex I (IPCC): <i>Total GHG emissions including LULUCF/LUCF - (Energy + Industrial Processes)</i> Annex I (CRF): <i>Total national emissions and removals) - (Energy + Industrial Processes and Product Use)</i>
CH ₄	<i>Anthropogenic</i>	<i>Fossil + Agriculture & Waste + Biofuel Burning</i>	Energy + Industrial Processes + Agriculture + Waste + Biofuel Burning*
	<i>Fossil</i>	<i>Fossil</i>	Energy + Industrial Processes - Biofuel Burning*
	<i>Agriculture and Waste</i>	<i>Agriculture & Waste</i>	Agriculture + Waste - Field burning of agricultural residues**
N ₂ O	<i>Anthropogenic</i>	Total - pre-industrial inland waters	Agriculture + Waste direct + anthropogenic indirect emissions (AIE = anthropogenic N leached to inland waters + anthropogenic N deposited from atmosphere) + energy and industry

2.7 Choice of example countries for analysis

370 For the analysis, we selected 12 countries (or groups of countries) based on specific criteria for each aggregated sector. Firstly, each chosen country had to possess a sufficiently large land area, as the limitations of coarse-spatial-resolution inversions make it difficult to reliably estimate GHG budgets for smaller countries. Additionally, it was preferable for the selected countries to have some coverage provided by the in situ global network of monitoring stations.

For CO₂, we focus on the land CO₂ fluxes of large fossil fuel CO₂ emitters. Although inversions do not allow to verify fossil 375 emissions in these countries as they are used as a fixed prior map of emissions, it is crucial to compare the magnitude of national land CO₂ sinks with fossil fuel CO₂ emissions in those large emitters. It is important to note that fitting net fluxes to changes in atmospheric CO₂ and then subtracting the prior fossil fuel (FF) fluxes can result in errors in the residual values, which are typically attributed exclusively to the sum of all non-FF fluxes. Additionally, we included two large boreal forested countries (Russia - RUS and Canada - CAN), two tropical countries with large forest areas (Brazil - BRA and the Democratic 380 Republic of Congo - COD), two large countries with ground-based stations (Mongolia - MNG and Kazakhstan - KAZ), and two large dry Southern Hemisphere countries also with high rankings in fossil fuel CO₂ emissions (South Africa - ZAF and Australia - AUS), both of which possess atmospheric stations to constrain their land CO₂ flux.

For CH₄, we first ranked countries (or groups of countries) based on their total anthropogenic, fossil, and agricultural emissions. This study includes China (CHN), India (IND), the United States (USA), the European Union (EUR), Russia (RUS), Argentina



385 (ARG) and Indonesia (IND), all of which are among the top emitters of both fossil fuel and agricultural CH₄ and possess large areas. Criteria of large land areas and the presence of atmospheric stations is crucial for in situ inversions. The advantage of utilizing GOSAT in CH₄ atmospheric inversions is its ability to provide observations over countries where surface in-situ data are sparse or absent, such as in the tropics. This allows us to consider countries with limited or few ground-based observations. Small countries were excluded due to the coarse spatial resolution. However, among the selected countries, Venezuela, with
 390 an area of 916,400 km², was chosen specifically for the analysis of CH₄ emissions. Despite being relatively small, Venezuela is a large emitter of oil and gas, potentially allowing for inversions using GOSAT satellite observations to constrain its emissions. In major oil- and gas-extracting countries that have negligible agricultural and wetland emissions like Kazakhstan (KAZ), grouped in this study with Turkmenistan (TKM) into KAZ&TKM; Iran (IRN); and Persian Gulf countries (GULF), fossil emissions should be easier to separate by inversions and thus to be compared with NGHGs.

395 For N₂O, we selected the top 12 emitters based on the NGHGs reports. Anthropogenic N₂O emissions in most of these countries are predominantly driven by the agricultural sector, which accounts for a share (including indirect emissions) ranging from 6% in Venezuela (VEN) to 95% in Brazil (BRA) of their total NGHGs emissions.

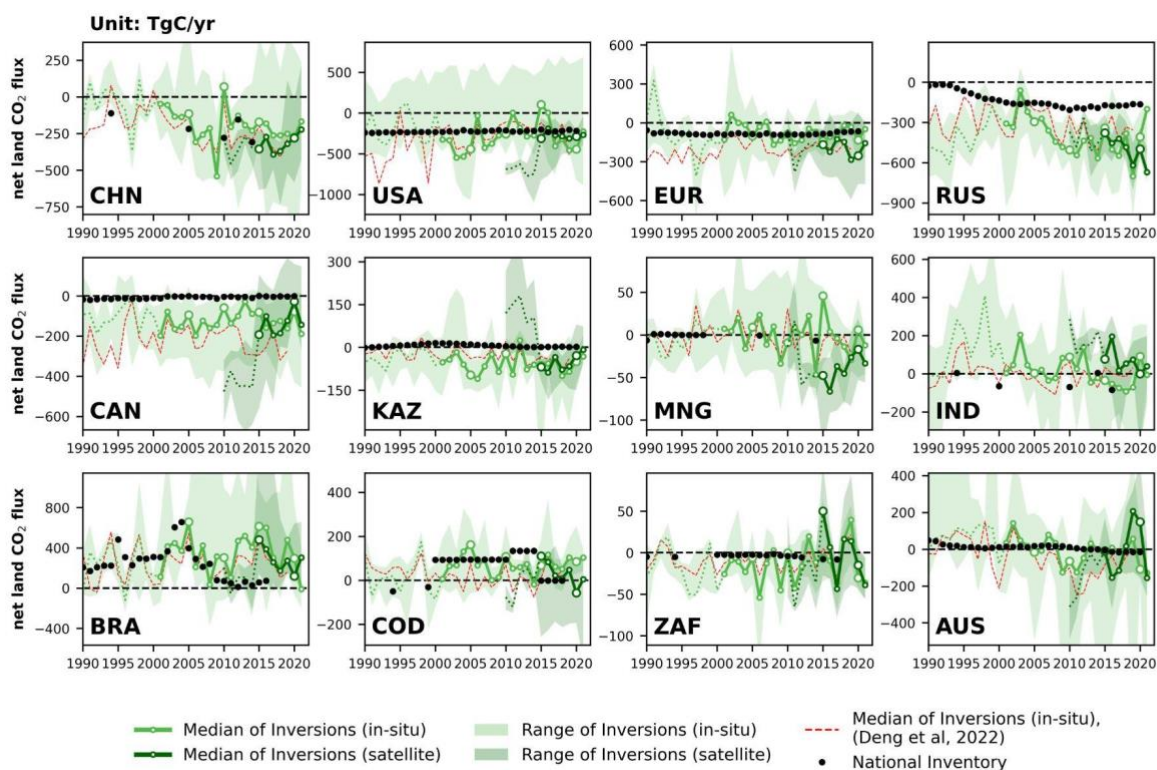
Together, the selected countries (or groups of countries) with a different selection for each gas, account for more than 90% of the global land CO₂ sink, 60% of the global anthropogenic CH₄ emissions (around 15% of fossil fuel emissions and
 400 approximately 40% of agriculture and waste emissions separately), and 55% of the global anthropogenic N₂O emissions, as estimated by the NGHGs.

Table 3. Lists of countries or groups of countries are analyzed and displayed in the result section for each aggregated sector. Argentina (ARG), Australia (AUS), BRA (Brazil), Bangladesh (BGD), Canada (CAN), China (CHN), Columbia (COL), Democratic Republic of the Congo (COD), Indonesia (IDN), India (IND), Iran (IRN), European Union (EUR), Kazakhstan (KAZ), Mexico (MEX),
 405 Mongolia (MNG), Nigeria (NGA), Pakistan (PAK), Russia (RUS), South Africa (ZAF), Sudan (SDN), Thailand (THA), United States (USA), Venezuela (VEN), GULF = Saudi Arabia + Oman + United Arab Emirates + Kuwait + Bahrain + Iraq + Qatar, KAZ&TKM = Kazakhstan + Turkmenistan. For CH₄, acronyms underlined denotes the countries appear in both *Anthropogenic* and *Fossil or Agriculture and Waste* sectors.

Gas	Super Sector	Country List
CO ₂	<i>Net Land Flux</i>	AUS, BRA, CAN, CHN, COD, EUR, IND, KAZ, MNG, RUS, USA, ZAF
CH ₄	<i>Anthropogenic</i>	<u>ARG</u> , AUS, <u>BRA</u> , <u>CHN</u> , <u>EUR</u> , <u>IDN</u> , <u>IND</u> , <u>IRN</u> , <u>MEX</u> , <u>PAK</u> , <u>RUS</u> , <u>USA</u>
	<i>Fossil</i>	<u>CHN</u> , <u>EUR</u> , GULF, <u>IDN</u> , <u>IND</u> , <u>IRN</u> , KAZ&TKM, <u>MEX</u> , NGA, <u>RUS</u> , <u>USA</u> , VEN
	<i>Agriculture and Waste</i>	<u>ARG</u> , BGD, <u>BRA</u> , <u>CHN</u> , <u>EUR</u> , <u>IDN</u> , <u>IND</u> , <u>MEX</u> , <u>PAK</u> , <u>RUS</u> , THA, <u>USA</u>
N ₂ O	<i>Anthropogenic</i>	AUS, BRA, CHN, COD, COL, EUR, IDN, IND, MEX, SDN, USA, VEN



3 Results for net land CO₂ fluxes



410

Figure 3 | Net land CO₂ fluxes (unit: TgC yr⁻¹) during 1990-2021 from China (CHN), United States (USA), European Union (EUR), Russia (RUS), Canada (CAN), Kazakhstan (KAZ), Mongolia (MNG), India (IND), Brazil (BRA), Democratic Republic of the Congo (COD), South Africa (ZAF), and Australia (AUS). By convention, CO₂ removals from the atmosphere are counted negatively, while CO₂ emissions are counted positively. The black dots denote the reported values from NGHIGIs. The light green color denotes the in-situ-alone CO₂ inversion (n=5) set while the dark green color denotes the set that uses satellite data (n=4). The green lines denote the median of land fluxes over managed land of CO₂ inversions, after adjustment of CO₂ fluxes from lateral transport by rivers, crop, and wood trade. When all inverse models within the inversion sets (in-situ: n=5; satellite: n=4) have available data for the same time interval, their median values are depicted as solid green lines. Otherwise, when the inversion sets have incomplete inverse models within the time interval (in-situ: n<5; satellite: n<4), their median values are represented as dashed green lines. The shading area denotes the min-max range of inversions. The red dashed lines denote the median of inversions presented by the previous study (Deng et al., 2022).

415

420

Fig 3 presents the time series of land-to-atmosphere CO₂ fluxes for the selected countries listed in **Table 2**. The median of inversions across the 12 countries shows significant interannual variability, reflecting the impact of climate variability on terrestrial carbon fluxes and annual variations of land-use emissions.

425

The adjustments of lateral CO₂ flux generally tend to lower land carbon sinks or increase land carbon emissions, especially in CHN, USA, EUR, RUS, CAN, IND, and BRA. However, even with these adjustments, in countries of temperate latitudes, the median values of the five in-situ-alone inversion ensemble all indicate a net carbon sink during the 2010s, such as CHN with



a median sink of 180 ± 100 TgC/yr, USA (210 ± 180 TgC/yr), EUR (90 ± 50 TgC/yr), RUS (490 ± 100 TgC/yr) and CAN (110 ± 40 TgC/yr). In CHN, despite only 5 reported values to UNFCCC, NGHGs show a good agreement with the inversion results, with both NGHGs and inversions exhibiting an overall increase in carbon sink over the study period. However, during
430 2015-2021, the median values of the satellite-based inversion ensemble show a higher carbon sink of 320 ± 60 TgC/yr than those from in-situ inversion results (220 ± 50 TgC/yr) in CHN. In IND, there are also only five reported estimates from the NGHGs. The in-situ inversion results indicate that India exhibited fluctuations between being a carbon source and a carbon sink during the period of 2001-2014 (40 ± 70 TgC/yr). During 2015-2019, the in-situ inversion results in IND show a median carbon sink of 65 ± 20 TgC/yr, however, the median reverted to being a carbon source of 91 TgC/yr (ranging from a sink of
435 350 to a source of 260) in 2020. In contrast, the median values of satellite-based inversion ensemble indicate a carbon source of 65 ± 60 TgC/yr during 2015-2021 in IND.

As Annex I countries, USA, EUR, RUS, CAN, and KAZ have continuously reported annual NGHGs since 1990. The NGHGs reported values for the USA and CAN indicate a decline trend (Mann-Kendall $Z=-0.6$, $p<0.01$) of carbon sinks by an annual average rate of 0.7 TgC/yr² and 0.5 TgC/yr². Like in Deng et al. 2022, we found that the carbon sink of Canada's managed
440 land is significantly larger (-125 ± 45 TgC/yr over 2001-2021 from in-situ inversions) than the NGHGs reports (5 ± 4 TgC/yr over 2001-2021). Part of this difference could be due to the fact that Canada decides in its inventory not to report fire emissions as they are considered to have a natural cause. Doing so, Canada also excludes recovery sinks after burning and those recovery sinks could surpass on average fire emissions, although remote sensing estimates of post fire biomass changes suggest that fire emissions have exceeded regrowth on average in Western Canada and Alaska until ≈ 2010 (Wang et al.,
445 2021). One reason for the difference may be that the NGHGI used old growth curves for forests, potentially underestimating the actual forest growth; Another reason for the difference may be shrubland and natural peatland carbon uptake and possibly an underestimated increase of soil carbon in the national inventory. For the USA we have a good agreement between inversions (-290 ± 180 TgC/yr for in-situ over 2001-2021) and the NGHGs data (-220 ± 10 TgC/yr over 2001-2021) with the inversion showing much more interannual variability, the US being a net source of carbon in the years 2011, 2015 and 2016 from the
450 median of in-situ inversions. The lower variability in the NGHGs data reflects the 5-years averaging of C stock changes by the national forest inventory. In EUR, the new in-situ inversion ensemble gives a lower carbon sink than the previous one (red line in Fig 3, see discussion in section 6.1), now being in good agreement (-75 ± 60 TgC/yr) with NGHGs (-85 ± 10 TgC/yr) over 2001-2021. The OCO₂ satellite inversions give a higher sink than in-situ inversions by -200 ± 85 Tg C/yr, possibly because the in-situ surface network does not cover Eastern European countries which have a larger NEE than Western
455 European ones, whereas OCO₂ data have a more even coverage of the continent, as discussed by Winkler et al. (2023) (see their Fig. 2 showing that OCO₂ inversions have a similar NEE than in-situ ones in Western Europe but a larger mean NEE uptake in Eastern Europe).

In contrast, the NGHGs in RUS reports a rapid trend of increasing sink by a rate of 4.6 TgC/yr² (Mann-Kendall $Z=0.69$, $p<0.01$) during 1990-2020, supported by the significant strong correlation with the medians of in-situ inversion ensemble



460 ($\rho=0.7$, $p<0.01$) during 2001-2020. However, the median values for both the in-situ (480 ± 100 TgC/yr) and satellite-based
(450 ± 90 TgC/yr) inversion ensemble over RUS indicate larger larger land carbon sinks than those reported in the NGHGs
(178 ± 11 TgC/yr) during 2011-2020. For KAZ, the NGHGs suggest that managed land is a slight carbon source (6 ± 5
TgC/yr) during 2000-2020. However, the median values for both satellite-based and in-situ inversion ensemble indicate a
465 carbon sink of 53 ± 29 TgC/yr and 57 ± 33 TgC/yr, respectively, during 2015-2021 and 2001-2021. It is worth noting that the
satellite-based inversion results for USA, CAN, and KAZ all exhibit shifts in their fluxes between 2010 and 2015 compared
to the results after 2015. This is attributed to the use of different satellite data and the number of different ensembles during
these periods. Before 2015, only GOSAT was available, and only 2 out of 4 systems were available. After the OCO-2 record
started, in September 2014, the satellite-driven inversion set only assimilated OCO-2. This indicates that inversion results
based on GOSAT data are not consistent at the country scale with OCO-2 inversions. As a result, we can compare OCO-2
470 inversions with NGHGs since 2015, but not the trends from inversions using GOSAT and/or OCO-2 inversions since 2009.
In BRA, both the NGHGs reports (239 ± 166 TgC/yr during 1990-2016) and inversion results (in-situ: 350 ± 190 TgC/yr
during 2001-2021; satellite-based: 280 ± 120 TgC/yr during 2015-2021) indicate that the country has been a net carbon source
since 1990. The carbon source from managed land in Brazil increased from the late 1990s, reaching a peak around 2005
according to NGHGs (677 TgC/yr). This evolution is confirmed by in-situ inversions with a source peaking in 2005 (~ 650
475 TgC/yr). The net carbon source from inversions then decreased from 2005 to 2011, which is consistent with the observed
reduction in deforestation due to forest protection policies implemented by the Brazilian government. This is an encouraging
result as the inversions did not explicitly consider land use emissions in their prior assumptions, although some included an
estimate of carbon released by fires in their prior which is part of land-use emissions in Brazil. Since NEE is defined as all
land fluxes except fossil fuel emissions, NEE from all inversions nevertheless include land use emissions from deforestation,
480 degradation emissions and fire emissions including fires from deforestation, degradation and other fires. After 2011, inversions
show a new increase in land emissions, with a peak during the 2015-2016 El Niño drought. There have been higher average
land emissions thereafter. These ongoing changes may be attributed to various factors such as the legacy effects of drought
leading to increased tree mortality (Aragão et al., 2018), higher wildfire emissions (Naus et al., 2022; Gatti et al., 2023), carbon
losses from forest degradation, and climate change-induced reductions in forest growth due to regional drying and warming in
485 the southern and eastern parts of the Amazon (Gatti et al., 2021). From 2011 to 2016, the NGHGs reports indicate that carbon
emissions from Brazilian managed lands were stable at around 47 TgC/yr. However, the medians of in-situ inversions suggest
that carbon emissions rapidly increased from ~ 100 TgC/yr in 2011 to ~ 600 TgC/yr in 2016, which peaked in 2015 (~ 610
TgC/yr). From 2016 to 2021, the medians for both in-situ and satellite inversion results show a decrease in carbon emissions
from 2016 to 2018 but a transient peak in 2019, a year with large fires (Gatti et al., 2023) (in-situ: 480 TgC/yr; satellite: 270
490 TgC/yr). Then carbon emissions decreased again until 2021, which experienced wetter conditions and fewer fires (Peng et al.,
2022); The in-situ inversion results show a continuous decrease to -10 TgC/yr in 2021, while the satellite inversion results
showed a persistent source carbon anomaly of 300 TgC/yr. We emphasize moreover that available CO₂ observations from a
network of aircraft vertical sampling (Gatti et al., 2021) were not used to constrain the inverse models used here.



For COD, the available NGHGs data indicates that before 2000, the country's managed lands were a net carbon sink (50
495 TgC/yr in 1994 and 30 TgC/yr in 1999). Since 2000, the NGHGs reports indicated three stages of different levels of CO₂ flux,
which COD managed land was a carbon source during 2000-2010 (95 ± 0.5 TgC/yr), a larger carbon source during 2011-2014
(135 ± 0.1 TgC/yr), and a very small sink during 2015-2018 (-1.2 ± 0.1 TgC/yr). The medians of in-situ inversion ensemble
indicate a similar annual average carbon source (70 ± 45 TgC/yr) during 2001-2021 with the NGHGs, despite the few
observations over Africa (Byrne et al., 2023). In the recent decade, satellite inversion results from 2015 to 2021 indicate a
500 smaller source (30 ± 55 TgC/yr) compared to the in-situ results (85 ± 25 TgC/yr). Moreover, the satellite inversion results
indicate a sink anomaly in 2020 (-60 TgC/yr) which is not found in the in-situ inversions. The sink anomaly in 2020 from the
satellite inversions is consistent with wetter conditions during that year over COD.

For ZAF, the NGHGs show a stable very small sink of 3 TgC/yr during 1990-2010 that doubled from 4 TgC/yr in 2010 to 8
TgC/yr in 2017, while the in-situ inversion results indicate large fluctuations from a carbon sink (especially peaked in 2006,
505 2009, 2011, 2017 and 2021) to a small carbon source (e.g., in 2013, and 2018-2019). From 2015 to 2021, the satellite-based
inversion results are consistent with the in-situ results for annual variability ($\rho=0.8$, $p<0.05$), which is a good sign of the
consistency between different atmospheric observing systems. During the transition to El Niño conditions and drought from
2014 to 2015, however, the satellite-based inversion results indicate a switch from a carbon sink to a source anomaly of 50
TgC/yr in ZAF which is not seen in the in-situ inversions.

In AUS, the NGHGs data shows a land source of carbon from 1990 to 2012, which decreased over time (from 48 TgC/yr in
1990 to 1 TgC/yr in 2012) and changed into a carbon sink since 2013 (that increased from a sink of 1 TgC/yr in 2013 to 15
TgC/yr in 2020). However, the in-situ inversions indicate fluctuations between a carbon source and a sink with an annual
average small sink of 10 ± 71 TgC/yr observed over the period of 2001-2021, except for 2009-2011, the medians of in-situ
inversions reveal a strong carbon sink of 105 ± 35 TgC/yr. Between 2010 and the strong La Niña year of 2011, the medians of
515 in-situ inversion ensemble from the previous study (Deng et al., 2022) showed an increase in carbon uptake of 145%. This
high carbon sink persisted in 2012, which was a dryer year with maximum bushfire activity. However, in this study, the
medians of updated in-situ inversion ensemble indicate that there is a sink anomaly in 2011 followed by a source anomaly in
2013, which appears to be more realistic. 2019 was the driest and hottest year recorded in Australia, including extreme fires at
the end of 2019 (Byrne et al., 2021). As a result, the medians for both in-situ and satellite inversion ensemble show a carbon
520 source anomaly in 2019, with 55 TgC/yr (ranging from a sink of 1060 to a source of 480) and 200 TgC/yr (ranging from a sink
of 120 to a source of 320) respectively. When it comes to the wet La Niña year of 2021, the medians for both in-situ and
satellite inversion ensemble indicate that AUS managed land became a carbon sink of 130 TgC/yr (ranging from a sink of
1120 to a source of 25) and 150 TgC/yr (ranging from a sink of 260 to a source of 40).

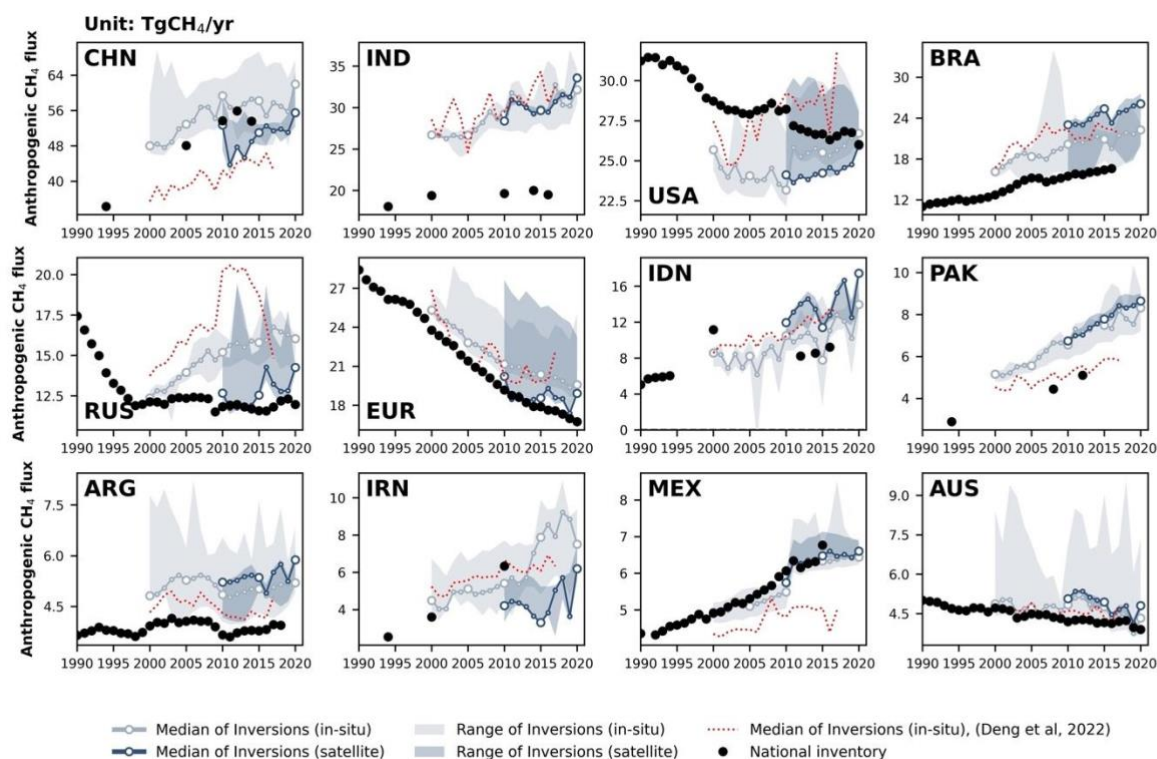
Last, we give the global comparison between NGHGs and inversions, using NGHGs data compiled for all countries by Grassi
525 et al. (2023) which include Annex I countries reports, non-Annex I NC, BUR and NDCs. The river correction is the only one
that changes the global NEE, because the global mean of CO₂ fluxes from wood and crop products is close to zero. The river-
induced CO₂ uptake over land that is removed from inversion NEE is equal to the C flux transported to the ocean at river



mouths (0.9 GtC/yr in our estimate, close to the value of Regnier et al. 2022). The (in-situ) inversions without the river correction give a global NEE sink of 1.8 GtC/yr over 2001-2020, managed land: 1.3 GtC/yr (72% of total), unmanaged land: 0.5 GtC/yr (28%). The in-situ inversions with the river correction study give a global NEE sink of 0.91 GtC/yr, managed land: 0.51 GtC/yr (56% of total), unmanaged land 0.4 GtC/yr (44% of the total) This is an important update from Deng et al. 2022 where the river CO₂ flux correction was not applied separately to managed / unmanaged lands. Because managed lands have a much larger area than unmanaged ones and because of the spatial patterns of the CO₂ sinks in the river correction are distributed with MODIS NPP which has low values in unmanaged lands of northern Canada and Russia, the river correction reduces strongly the C storage change with respect to NEE over managed lands, and marginally in unmanaged lands.. Inventory data recently compiled by Grassi et al. (2023) indicates a similar global land sink (on managed land) of 0.53 GtC yr⁻¹ with gap-filled data during the same period than the inversions with our improved river correction.

4 Results for anthropogenic CH₄ emissions

4.1 Total anthropogenic CH₄ emissions



540

Figure 4. Total anthropogenic CH₄ fluxes for the 12 top emitters: China (CHN), India (IND), United States (USA), Brazil (BRA), Russia (RUS), European Union (EUR), Indonesia (IDN), Pakistan (PAK), Argentina (ARG), Iran (IRN), Mexico (MEX), and



Australia (AUS). The black dots denote the reported values from NGHGs. The light and dark blue lines/areas denote the median and maximum-minimum ranges of in-situ and satellite-based CH₄ inversions based on EDGARv6.0 as the prior respectively.

545 **Fig 4** presents the variations in anthropogenic CH₄ emissions for the 12 selected countries, where these emissions are summing the sectors of agriculture and waste, fossil fuels, and biofuel burning. The distribution of emissions is highly skewed even among the top 12 emitters, with the largest and most populated countries such as CHN, IND, USA, BRA, RUS, and EUR which emits more than 10 TgCH₄/yr annually, while other countries have smaller emissions (ranging from 3 to 10 CH₄/yr) that are more challenging to quantify through inversions. During 2010-2020, CHN has the highest total anthropogenic emissions

550 at around 50 ± 3.5 Tg CH₄/yr, followed by IND with 30 ± 1.4 Tg CH₄/yr, USA with 24 ± 0.6 Tg CH₄/yr, BRA with 24 ± 1.2 Tg CH₄/yr, EUR with 19 ± 0.7 Tg CH₄/yr, IDN with 14 ± 0.9 Tg CH₄/yr and RUS with 13 ± 0.9 Tg CH₄/yr, according to the medians of satellite-based inversion ensemble based on EDGARv6.0 as prior. The remaining countries have emissions of approximately 5 Tg CH₄/yr. In general, the difference between NGHGs and inversions aligns in the same direction based on

555 observations are independent from in situ networks. Overall, satellite-based inversions may be more robust across most countries due to better observation coverage, except in EUR and the USA where the in-situ network is more extensive. Developing countries, such as CHN, IND, BRA, IDN, PAK, IRN and MEX, show a rapid increase in anthropogenic CH₄ emissions supported by reported values from NGHGs and results from inversions. In CHN, the reported values from NGHGs (when available) generally align with the results obtained through inversions (e.g., during 2010-2015, NGHGs: 54 ± 1.3 Tg

560 CH₄/yr, in-situ: 58 ± 1.2 Tg CH₄/yr, satellite-based: 48 ± 3.4 Tg CH₄/yr). During 2010-2020, the median values for the in-situ and satellite-based inversion ensemble show a similar increase trend at an annual growth rate of 0.28 Tg CH₄/yr² and 0.26 Tg CH₄/yr² respectively, although the medians of in-situ inversion ensemble (58 ± 2.0 TgCH₄/yr) were slight higher than the satellite-based ensemble (50 ± 3.5 TgCH₄/yr). However, in 2020, the medians of the emission estimates for both in-situ and satellite-based inversions reveal a rapid increase by 9% and 11% compared to 2019 in CHN, indicating a possible surge in

565 anthropogenic methane emissions for that year, possibly an artifact from the fact that the decreased OH sink in 2020 is not well accounted for here. Indeed OH IAV were not prescribed to all inversions, and when accounted for the OH IAV prescribed (based on Patra et al., 2021) was much smaller than those suggested by recent studies (e.g., Peng et al., 2022). As a result overestimating the sink in the inversions leads to overestimated surface emissions. The surge in emissions could also be due to spin-down, the last six month to one year of inversions being less constrained by the observations, even though the inversion

570 period covered up to June 2021.

In IND, PAK and MEX, there is good agreement ($r > 0.8$, $p < 0.01$) between the in-situ and satellite-based inversion ensembles (respectively, 31 ± 1.2 Tg CH₄/yr and 30 ± 1.4 Tg CH₄/yr in IND, 8 ± 0.7 Tg CH₄/yr and 7 ± 0.5 Tg CH₄/yr in PAK, and 6 ± 0.2 Tg CH₄/yr and 6 ± 0.3 Tg CH₄/yr in MEX), while both of them present a significant increasing trend of anthropogenic methane emissions in these countries (Mann-Kendall $p < 0.05$). However, when comparing to NGHGs values, the inversion

575 results in IND and PAK indicate >50% larger emissions than the values reported from the NGHGs during 2010-2020. In contrast, values reported from the NGHGs (6 ± 0.2 Tg CH₄/yr) by MEX also show good agreement with the inversion results.



In BRA, IDN and ARG, the medians for in-situ and satellite-based inversion ensembles show good consistency ($r=0.8$, $p<0.01$) in these two countries, while satellite-based inversion results are generally higher than the in-situ inversion results. Specifically, in BRA, the satellite-based inversions (24 ± 1.2 Tg CH₄/yr) were 16% higher than the in-situ inversions (21 ± 0.8 Tg CH₄/yr) and 52% higher than the NGHGI estimation (17 ± 0.4 Tg CH₄/yr) during 2010-2020, possibly owing to difficulties for inversions to separate between natural (wetlands, inland waters) and anthropogenic sources in this country, and possible flaws in the prior used for natural and anthropogenic fluxes. In IDN, NGHGIs reported a significant continuous upward trend at an annual average growth of 0.3 TgCH₄/yr, with a noticeable positive outlier in 2000. The medians for both in-situ and satellite-based inversion ensembles also indicate an upward trend in IDN, but both of them present sudden dips in anthropogenic methane emissions in 2015 and 2019 by 15~23% and 16~25%, compared to the previous year respectively. It is unlikely that anthropogenic activities could contribute such large year to year variations except for different flooded areas used for rice paddies. In ARG, the satellite-based inversion results also indicate two sudden dips in 2016 and 2019, however, such pattern was not found in the in-situ inversion results. A cause of year to year variations from inversions is the lack of in-situ sites and variable cloud cover affecting the density of GOSAT data.

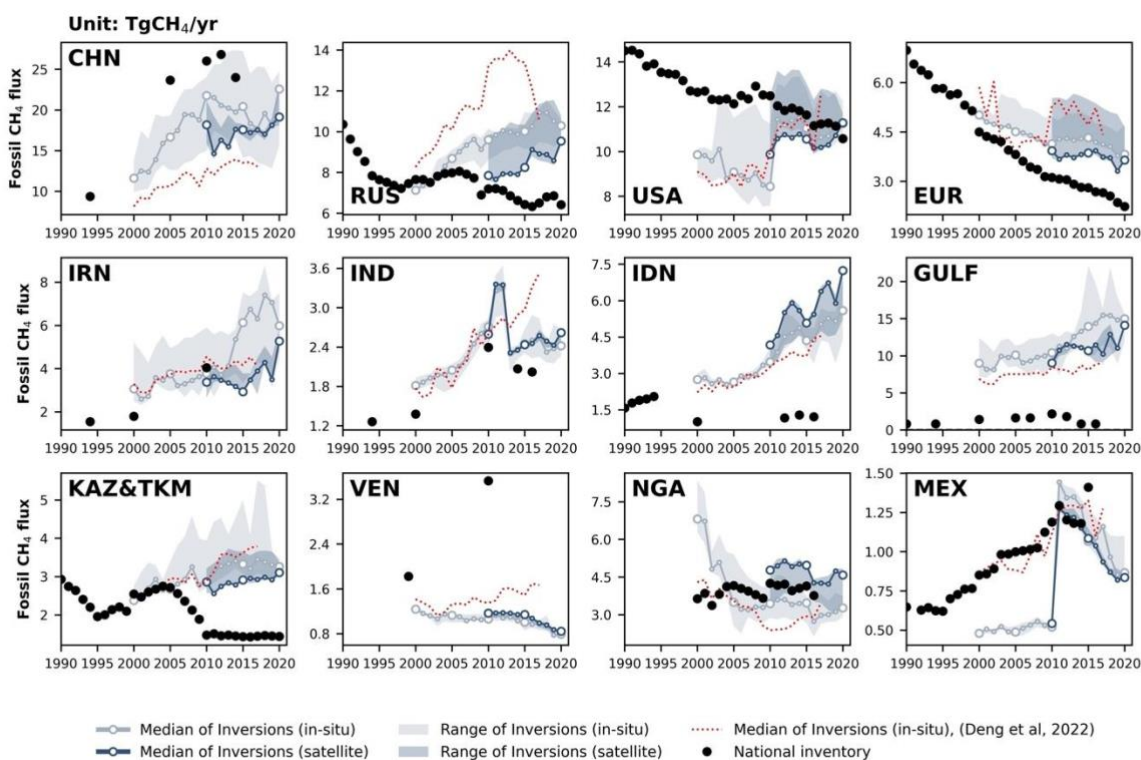
Regarding IRN, NGHGIs only provided data for three years (1994, 2000, and 2010), making it difficult to compare with inversion results. However, NGHGIs show a rapid growth in anthropogenic CH₄ emissions (+9.4%/yr) during this period. There are significant differences between inversion results and for IRN, with satellite inversions generally giving lower emissions than in-situ inversions and different trends. Satellite inversions suggest a declining trend between 2010 and 2015, followed by a fluctuating increase until 2020. In contrast, in-situ-based inversions (by any nearby measurement stations, thus likely reflecting the prior trend) show a rapid rise in emissions after 2010, reaching a peak in 2018, followed by a decline.

NGHGIs for RUS indicate that anthropogenic CH₄ emissions have been reduced during the 1990s and remained stable since 2000 (12.0 ± 0.3 Tg CH₄/yr during 2000-2020), which is similar with the trend observed from satellite-based inversion results (12.7 ± 0.9 Tg CH₄/yr during 2000-2020). However, in 2016, there was a sudden increase of emissions in satellite inversion results (+14% increase from 12.5 in 2015 to 14.2 Tg CH₄/yr in 2016), followed by a gradual decline, and then a new increase in 2020 (+11% increase from 12.8 Tg CH₄/yr in 2019 to 14.3 Tg CH₄/yr in 2020). This recent change was not observed in the in-situ inversion results or the NGHGIs.

For USA, AUS, and EUR, NGHGIs reported a slow declining trend (EUR: 0.4 Tg CH₄/yr; USA: 0.2 Tg CH₄/yr; AUS: -0.04 Tg CH₄/yr) in anthropogenic CH₄ emissions. In the case of the USA, inversion-derived emissions are slightly lower than NGHGIs (in-situ-based: 9.3% lower during 2000-2020; satellite-based: 11.4% lower during 2010-2020). However, both ground-based and satellite-based inversions indicate that anthropogenic CH₄ emissions have remained relatively steady since 2000, without reflecting the slow decline reported by NGHGIs. In EUR, NGHGIs indicate that anthropogenic CH₄ emissions have been decreasing rapidly since 1990 (-1.4%/yr), consistent with the trend obtained from inversion results. However, in-situ inversion emissions are on average slightly higher than NGHGIs, and this difference has been gradually increasing from 7.7% in the 2000s to 14.5% in the 2010s.



610 4.2 Fossil CH₄ emissions



615 **Figure 5.** CH₄ emissions from the fossil fuel sector from the top 12 emitters of this sector: China (CHN), Russia (RUS), United States (USA), European Union (EUR), Iran (IRN), India (IND), Indonesia (IDN), Persian Gulf countries (GULF = Saudi Arabia + Iraq + Kuwait + Oman + United Arab Emirates + Bahrain + Qatar), Kazakhstan & Turkmenistan (KAZ&TKM), Venezuela (VEN),
 620 Nigeria (NGA), and Mexico (MEX). The black dots denote the reported value from the NGHGs. In the NGHGI data shown in Fig 5 for GULF, Saudi Arabia reported four NGHGs in 1990, 2000, 2010, and 2012, Iraq reported one in 1997, Kuwait reported three in 1994, 2000, and 2016, Oman reported one in 1994, United Arab Emirates reported four in 1994, 2000, 2005 and 2014, Bahrain reported three in 1994, 2000 and 2006, and Qatar reported one in 2007. The reported values are interpolated over the study period to be summed up and plotted in the figure. For KAZ&TKM, the reported values of Turkmenistan during 2001-2003, 2005-2009, 2011-2020 are interpolated and added to annual reports from Kazakhstan, an Annex I country for which annual data are available. Other lines, colors and symbols as **Fig 4**.

Fig 5 presents the fossil CH₄ emissions for the top 12 emitters from the fossil sector based on EDGARv6.0 as the prior. The largest emitter is CHN, mainly from the sub-sector of coal extraction, followed by RUS and USA. In CHN, the in-situ (20 ± 1.6 Tg CH₄/yr) and satellite inversions (17 ± 1.3 Tg CH₄/yr) emissions in the 2010s are 24% and 35% lower than in the NGHGs (26 ± 1.5 Tg CH₄/yr), respectively. The NGHGs in CHN suggest a decrease from 28 in 2012 to 24 TgCH₄/yr in 2014. However, both in-situ and satellite inversion results indicate an increasing trend since 2018. In IND and IDN, NGHGs report a decreasing trend during the study period, while inversions suggest a rapid increase in IDN and a stable value in IND after a peak in 2012. In IND, satellite inversions suggest a peak of fossil CH₄ emissions during 2011-2012, which then dropped

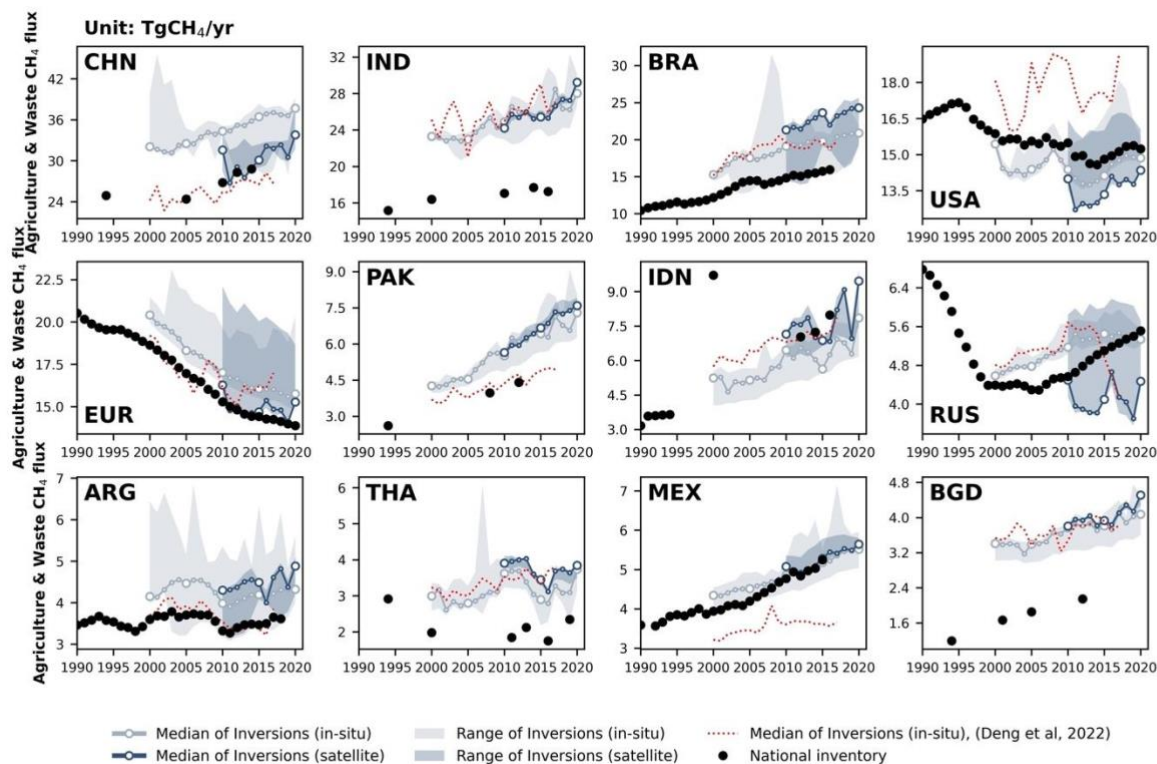


in 2013 and remained stable afterward. In IDN, both in-situ and satellite inversions indicate a fluctuating trend, with a significant drop between 2015 and 2019. In RUS, both in-situ and satellite inversion-based estimates of fossil fuel emissions are higher than NGHGs, and show an increasing trend, while NGHGs report a decreasing trend. This discrepancy may be due to inversion problems for separating between wetland emissions and gas extraction industries both located in the Yamal peninsula area, or leaks not captured in NGHGs. In USA, NGHGs overall show a significant declining trend (Mann-Kendall $Z=-0.8$, $p<0.01$). In-situ inversion estimates of fossil fuel emissions are 26% lower than NGHGs during 2000-2010, and remained consistent until around 2011. Nearly all in-situ inversions show a jump in fossil fuel emissions in 2011. In EUR, both NGHGs and inversion results demonstrate a consistent declining trend. However, starting from 2010, both in-situ and satellite inversions are higher than NGHGs reports.

Major oil-producing countries in the Persian Gulf are too small compared to the model resolution to be studied individually. Hence, NGHGs from the GULF countries (Saudi Arabia, Iraq, Kuwait, Oman, United Arab Emirates, Bahrain, and Qatar) were grouped and show much lower emissions compared to inversion results. In the 2010s, in-situ and satellite inversions estimate that emissions in GULF were 9 times and 8 times higher than the estimates reported in NGHGs, respectively. This huge under-reporting of emissions in GULF could be partly attributed to the omission of ultra-emitters in NGHGs. Indeed, recent studies by Lauvaux et al. (2022) have identified more ultra-emitters and larger emission budgets from ultra-emitters in Qatar, Kuwait, and Iraq. In KAZ&TKM, grouped together because of their rather small individual areas, both in-situ (3.3 ± 0.2 Tg CH_4/yr) and satellite (2.9 ± 0.1 Tg CH_4/yr) inversions estimate emissions to be 2 times higher than NGHGs (1.5 ± 0.1 Tg CH_4/yr) in the 2010s. Similarly, KAZ is located downwind of TKM, which has a high share of ultra-emitters. The global inversions operating at a coarse resolution may misallocate emissions from TKM to KAZ. It is worth noting that KAZ has two in-situ stations for CH_4 measurements, whereas the GULF countries lack in-situ station networks. On the other hand, the GOSAT satellite provides a dense sampling of atmospheric column CH_4 in the Persian Gulf region due to frequent cloud-free conditions. Therefore, GOSAT inversions can be considered more accurate than in-situ inversions for IRN, GULF countries, and KAZ&TKM. Additionally, it is important to note that GOSAT inversions generally give lower emissions than in-situ inversions in those countries. VEN is a rare case where NGHGs report much higher CH_4 emissions than inversions. While the uncertainty of GOSAT inversions (model spread) has decreased compared to the results reported by Deng et al. 2022, the gap between inversions and NGHGs has increased. In 2010, NGHGs reports of fossil CH_4 emissions in VEN were 298% higher than GOSAT inversions and 326% than in-situ inversions. We do not have a clear explanation for this large difference, except that VEN has strongly decreased oil and gas extraction due to sanctions curbing its crude production from 2.65 mb/d in 2015 to 0.57 mb/d in 2020 (OPEC, 2023), which may not be reflected in their NGHGs. In NGA and MEX, NGHGs estimates fall between the median of in-situ and satellite inversions during 2010-2020. However, in MEX, the in-situ inversion was 50% lower than NGHGs in the 2000s and showed a sudden large increase in 2010.



4.3 Agriculture and waste CH₄ emissions



660

Figure 6. CH₄ emissions from agriculture and waste for the 12 largest emitters in this sector, China (CHN), India (IND), Brazil (BRA), United States (USA), European Union (EUR), Pakistan (PAK), Indonesia (IDN), Russia (RUS), Argentina (ARG), Thailand (THA), Mexico (MEX), and Bangladesh (BGD). The black dots denote the reported estimates from NGHGs. Other lines, colors, and symbols as Fig 4.

665 **Fig 6** presents CH₄ emissions of the Agriculture and waste sector for the top 12 emitters of this sector. In all countries except for the USA and RUS, the values reported by NGHGs are systematically lower than the inversion results. The results from the previous ensemble of in-situ inversions (red dotted line) are consistent with those of the inversions used in this study except in the USA where previous inversions are 3.2 TgCH₄/yr higher, in RUS where they show a drop after 2015 although they remain in the range from the new satellite and in-situ inversions, and in MEX where they are systematically lower by 1.6

670 TgCH₄/yr.

In CHN, the most recent NGHGs reports in 2012 and 2014 estimate agriculture and waste emissions at 28 Tg CH₄/yr, which is close to satellite inversions (28 ± 1 TgCH₄/yr) but 22.4% lower than the median in-situ inversions (35 ± 0.5 TgCH₄/yr) and closer to their minimum value. The trend in agricultural and waste emissions is consistent between inversions and NGHGs for CHN. In IND, inversions consistently show higher emissions than NGHGs by approximately 50% and indicate an

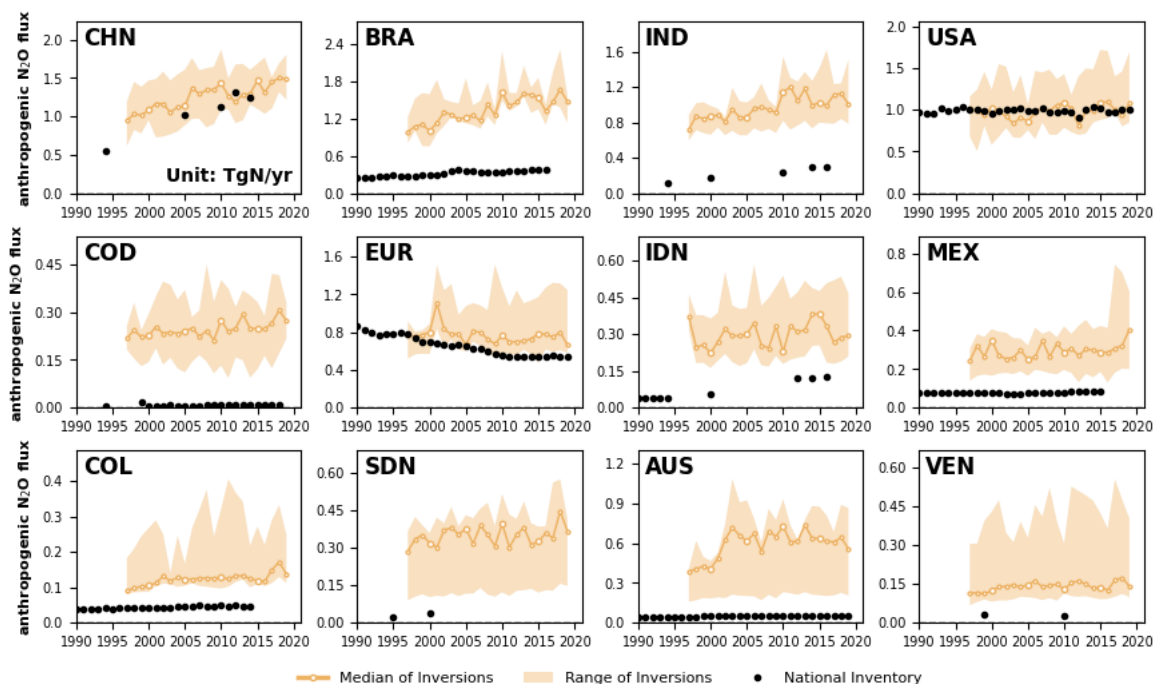
675 increasing trend during 2000-2020, whereas the NGHGI last communication being for 2016, it does not allow us to give a



recent trend. According to the national inventory of IND, enteric fermentation is the primary source of CH₄ emissions in the agriculture and waste sector, contributing 61% of emissions, with rice cultivation accounting for 20% and waste contributing 16%. A similar pattern is observed in BGD, where agricultural emissions are dominated by rice production (48% in 2012) and enteric fermentation (42% in 2012). Satellite and in-situ inversions estimate emissions in BGD are nearly double than those reported by NGHGs during 2001 and 2012, the last communication. The significant discrepancies between inversions and NGHGs in IND and BGD may be attributed to potential underestimation of livestock or waste CH₄ emissions by NGHGs. NGHGs utilized the Tier 1 method and associated emission factors from the 2006 IPCC Guidelines for National Greenhouse Gas Inventories (IPCC, 2006). However, a recent study (Chang et al., 2021) found that estimates using revised Tier 1 or Tier 2 methods from the 2019 Refinement to the 2006 IPCC Guidelines for National Greenhouse Gas Inventories (IPCC, 2019) give livestock emissions 48%-60% and 42%-61% higher for IND and BGD by 2010, respectively, compared to Tier 1 IPCC (2006) methods, which would bring bottom up emissions closer to inversions. In BRA, both satellite and in-situ inversions consistently estimate larger emissions than the NGHGs by 34% and 29%, respectively, and show a consistent increasing trend over their study periods. In the USA, the medians of satellite and in-situ inversions are slightly lower than those of NGHGs, but they exhibit a similar trend throughout the study period. The trend of inversions is comparable to the one of the NGHGs in BRA during their period of overlap, although there is no NGHGs communication later than 2016. In ARG, PAK and THA, the medians of in-situ inversions show good consistency with satellite inversion results. Nevertheless, in-situ inversion emissions in the 2010s are, on average, 47% higher in PAK, 20% higher in ARG, and 64% higher in THA compared to the NGHGs reports. In EUR, emissions from agriculture and waste were reported to have significantly decreased over time in the NGHGI data, mainly from solid waste disposal (Petrescu et al., 2021), a trend that is captured by inversions and is close to the one of the NGHGs over the study period. In contrast, emissions from agriculture and waste in RUS are reported to have a positive trend after 2010 by the NGHGI, with in-situ inversions producing a consistent trend from 2000 to 2014 but a sharp decrease thereafter, while satellite inversions are producing stable emissions, albeit lower than the NGHGs and in-situ inversions after 2010.



5 Results for anthropogenic N₂O emissions



700

Figure 7. Anthropogenic N₂O fluxes of the top 12 emitters: China (CHN), Brazil (BRA), India (IND), United States (USA), Democratic Republic of the Congo (COD), European Union (EUA), Indonesia (IDN), Mexico (MEX), Colombia (COL), Sudan (SDN), Australia (AUS), and Venezuela (VEN). The black dots denote the anthropogenic emissions from the UNFCCC national greenhouse gas inventories. The thick orange lines and the light orange areas denote the median and the maximum-minimum ranges of anthropogenic fluxes respectively among all N₂O inversions. We restricted our analysis to data starting from 1997 because it was the year

705

when data from the all four inversion models are available. We present the 12 countries/regions with the largest anthropogenic N₂O emissions in the world (Fig 7), which in total contribute approximately 55% of global anthropogenic N₂O emissions. The estimates from both NGHGI and inversions in CHN, USA, and EUR demonstrate a relatively close match between NGHGI and inversions (in-situ only). These three large emitting countries/regions exhibit different trends in their anthropogenic N₂O emissions. In CHN, both NGHGI and inversions indicate an increasing trend in anthropogenic N₂O emissions. In the USA, anthropogenic N₂O emissions seem to have reached a state of relative stability, with NGHGI and inversion results showing similar mean values and lack of trends. In EUR, both NGHGI and inversions show a declining trend in anthropogenic N₂O emissions, but from 2010 to 2020, the NGHGI estimates are lower (20%) than the median values derived from inversion models, that is, the negative trend from inversions is less pronounced than the one of NGHGI. Most other selected countries display higher anthropogenic N₂O emissions from inversions than from NGHGI (i.e., BRA, IND, COD, IDN, MEX, COL, SDN, VEN). These discrepancies in anthropogenic N₂O emissions are possibly attributable to factors that have been analyzed in our previous study (Deng et al., 2022). Firstly,

710

715

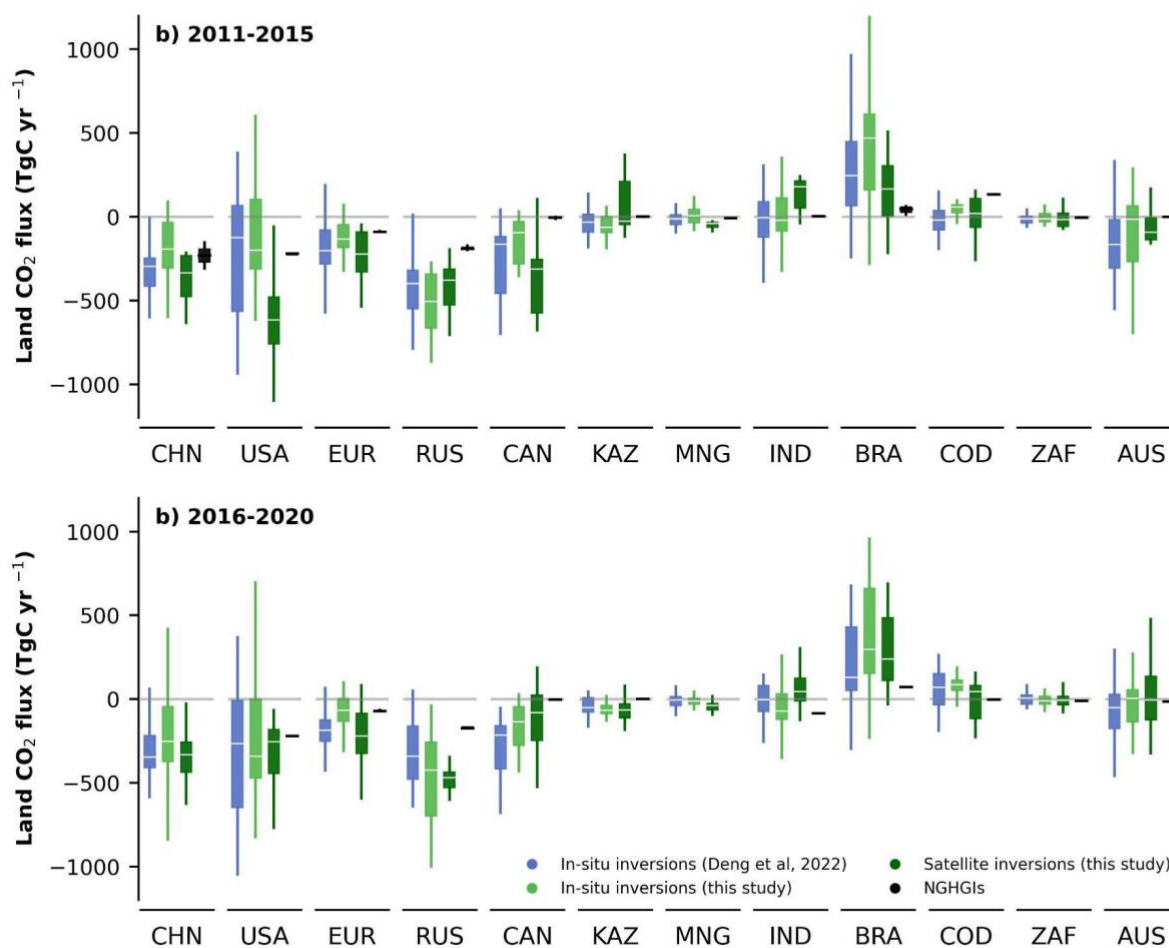


nearly all these non-Annex 1 countries utilize Tier 1 emission factors (EFs), which may underestimate emissions n when soil and climate dependence is taken into account (Cui et al., 2021). This has been noted in previous studies (Philibert et al., 2013; 720 Shcherbak et al., 2014; Wang et al., 2020). Furthermore, the observed concave response of cropland soil emissions as a function of added N fertilizers may also contribute to underestimated emissions in NGHGs, as the relationship is non-linear and higher than the linear relation used by NGHGs in Tier 1 approaches (Zhou et al., 2015). In an improved reporting framework, EFs should also account for both natural and anthropogenic components, as they cannot be distinguished through field measurements, from which EFs are derived. However, in practice, EFs are mostly based on measurements made in temperate 725 climates and soils from established croplands with few "background" emissions. Consequently, there could be a systematic underestimation of default IPCC EFs from tropical climates and for recently established agricultural lands, for which the IPCC EFs also have a huge uncertainty of up to $\pm 75\%$ – 100% . Another factor that might contribute to the discrepancy is the omission of emissions from reactive nitrogen contained in organic fertilizers (manure), for which NGHGs do not provide specific details for non-Annex 1 reports. Lastly, anthropogenic indirect emissions (AIEs) from atmospheric nitrogen deposition and leaching 730 of human-induced nitrogen additions to aquifers and inland waters are reported by Annex 1 countries using simple emission factors, but non-Annex 1 countries do not consistently report AIE. However, in AUS, the gap between inversions and NGHGs is even expanded compared to our previous study. We do acknowledge that the density of the N_2O in-situ network in tropical countries and around AUS is so low that inversions most likely are attracted to their priors. The use of a lower prior could thus also be consistent with scarce atmospheric observations, and we have only a low confidence on N_2O inversion results for 735 tropical countries and AUS.



6 Discussion

6.1 Comparing net land CO₂ flux estimates from different inversion model ensembles



740 **Figure 8.** Net CO₂ land fluxes during the period of a) 2011-2015; and b) 2016-2020 in China (CHN), United States (USA), European Union (EUR), Russia (RUS), Canada (CAN), Kazakhstan (KAZ), Mongolia (MNG), India (IND), Brazil (BRA), Democratic Republic of the Congo (COD), South Africa (ZAF), and Australia (AUS). Blue boxes denote the in-situ inversion results from Deng et al. (2022) processed from Global Carbon Budget 2020 (Friedlingstein et al., 2020). Light green boxes denote the in-situ inversion results processed in this study, while dark green boxes denote the satellite inversion results. Black boxes denote the NGHGIs reported values. The white lines in



745 the boxes denote the medians of the land CO₂ fluxes. Note that the inversion results here have been adjusted by the lateral flux before the comparison.

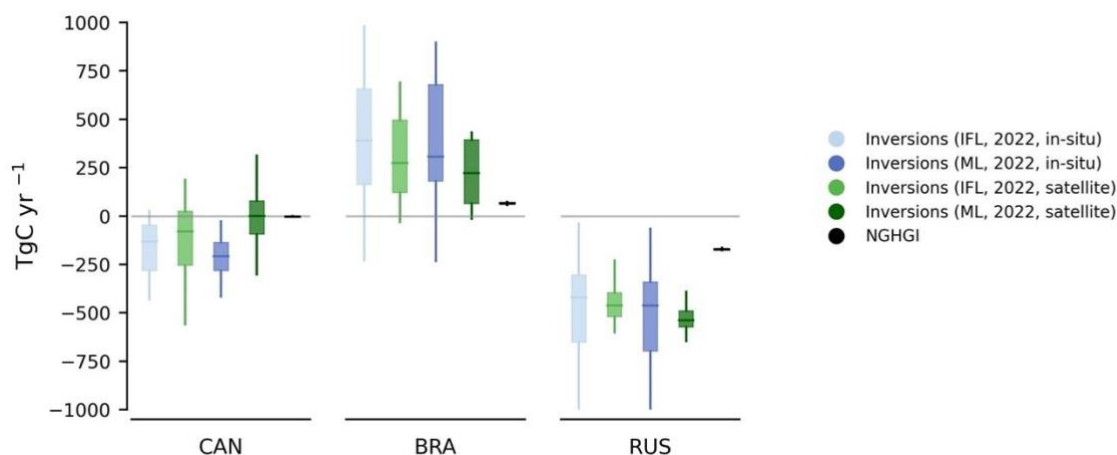
In this section, we compare four different estimates of land CO₂ fluxes during the period 2010-2020 (**Fig 8**), including: 1) medians of in-situ inversion results from our previous study (Deng et al., 2022), 2) medians of in-situ and 3) satellite-based inversion results processed in this study based on the Global Carbon Budget 2022 (Friedlingstein et al., 2022), and 4) NGHGs. This enables a comparison of the median and range of our in-situ inversion results (n=5) with those from previous study (n=6),
750 and assesses the performance differences between satellite-based (n=4) and in-situ inversion models. To ensure a fair comparison and avoid anomalies in the satellite-based inversion results during 2010-2015 when some of these inversions used GOSAT after 2010 and then OCO-2 after 2015, we separate the analysis into two periods: 2011-2015 and 2016-2020.

The variations of yearly land CO₂ fluxes span a comparable range between the current and previous in-situ inversion ensembles, indicating that consistency of the inversion results, but the uncertainty within the new in-situ inversion ensemble
755 was not improved. However, examining the median values, results from the new in-situ inversion ensemble may be closer to NGHGs in most countries (such as CHN, USA, EUR, CAN, KAZ, IND). This suggests that the new in-situ inversion ensemble used in this study has partially narrowed down the gaps between inversion results and NGHGs compared to the previous one. However, in RUS and BRA, the difference between the median of in-situ inversion ensembles and NGHGs has enlarged. For example, in RUS, median the new in-situ inversion ensemble indicate a larger carbon sink than those from Deng et al. (2022),
760 while the difference between median of in-situ inversions and NGHGs increases 51% during 2011-2015 (from 208 TgC/yr to 314 TgC/yr) and 49% during 2016-2020 (from 168 TgC/yr to 249 TgC/yr). Conversely, in BRA, median of the new in-situ inversion ensemble indicate a larger carbon source, while the difference increases over 100% during 2011-2015 (from 200 TgC/yr to 423 TgC/yr) and nearly 300% during 2016-2020 (from 56 TgC/yr to 223 TgC/yr).

As for the inversion ensemble used in this study, in most countries, the variations of yearly land CO₂ fluxes also span a similar
765 range between satellite-based inversion ensemble and in-situ inversion ensemble. However, in the cases of USA, RUS, CHN and BRA, the spread of satellite-based inversion results are narrower than those of in-situ inversion results, indicating a better consistency among available satellite-based inversion models, at least when similar satellite data are assimilated. In addition, in most cases, smaller difference were found between the median of inversion results and the NGHGs. For countries with dense surface monitoring networks such as in the USA and EUR, the satellite-based inversion results show good agreement
770 in-situ inversion results. However, for countries with sparse station coverage like KAZ and MNG, satellite-based inversion results could provide more reliable estimates due to more extensive spatial sampling from satellites, although the medians of satellite-based inversion results indicate larger carbon sinks and larger differences compared with NGHGs (than for in-situ inversion results). In USA and CAN, the difference during 2011-2015 (only GOSAT period) between in-situ and satellite-based inversion ensembles are larger than that during 2016-2020 (OCO₂ period). This can be attributed to the use of different
775 satellite data during these periods and different numbers of ensemble members. Before 2015, only GOSAT was available, and only 2 out of 4 systems. The inversion of OCO-2 data starting in 2014 result in a better alignment among OCO-2 ACOS v10 inversions, indicating the in-situ and satellite evaluations were similar (Byrne et al., 2023).



6.2 Adjustment of the national managed land masks to separate the net land CO₂ flux estimates



780 **Figure 9.** Net CO₂ land fluxes during the period of 2015-2020 in Canada (CAN), Brazil (BRA), and Russia (RUS). ‘IFL’ stands for
using the intact forest landscape data as a mask for non-managed land to extract land CO₂ flux from managed land and ‘ML’ indicates the
785 adjusted mask used by Grassi et al. (2023) to extract land CO₂ flux from managed land. The ‘in-situ’ stands for inversion results using
in-situ observations, and ‘satellite’ represents inversions using satellite observations. Note that the inversion results here have been adjusted by
the lateral flux before the comparison.

785 Following the method proposed by Grassi et al. (2023), we updated in this study the managed land mask for CAN and BRA
by using maps of managed land derived from NGHGI, and for RUS by adjusting tree-cover threshold in the tree cover map
from Hansen et al. (2013) to match the average area of managed land per Oblast (province) that is used for the NGHGIS.
Thus, the new mask is now more consistent with the definition of managed land in the NGHGIS for these three countries, so
790 in inversions (**Fig 9**). Generally, in Russia (RUS) and Canada (CAN), the managed land CO₂ fluxes extracted from the new
mask are closer to NGHGIS than those separated by the previous mask used by Deng et al. 2022. In addition, in Brazil (BRA),
adjusting the national managed land mask resulted in greater land carbon emissions, increasing the gap with NGHGIS.
However, the improvement of the managed land mask in this study is still not able to explain all the existing discrepancy
795 further analysis. We also observe in **Fig. 9** that the impact of our new managed land mask compared to the previous one, is
qualitatively similar whether it is applied to in-situ inversions or satellite inversions gridded flux fields.



6.3 Comparison of anthropogenic CH₄ emissions with Deng et al 2022

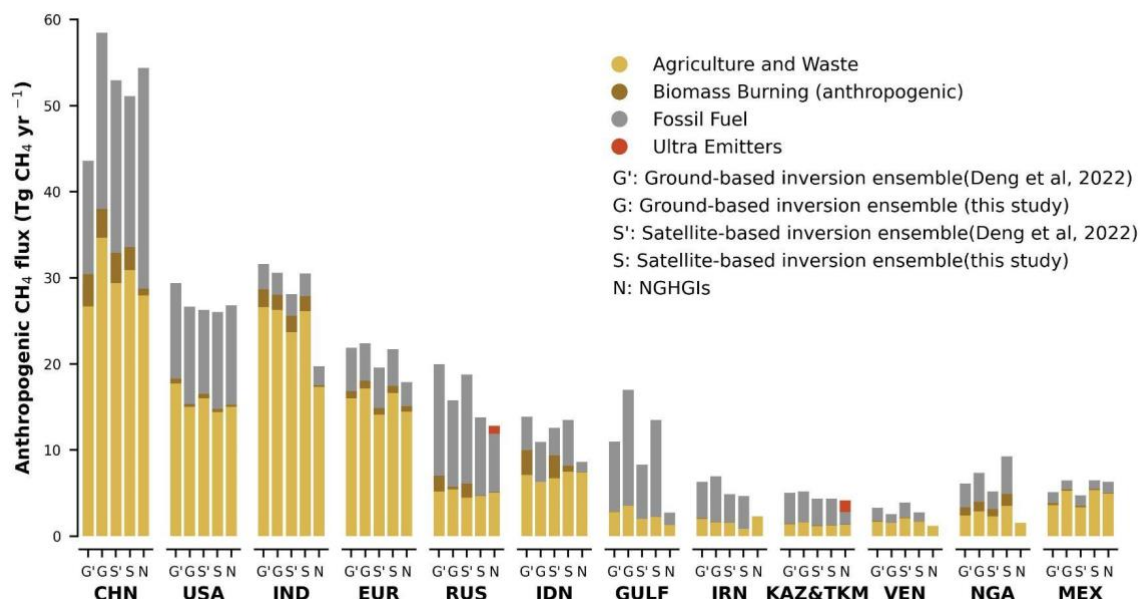


Figure 10. Annual average of anthropogenic CH₄ emissions from in-situ (G) and satellite (S) inversions and national greenhouse gas inventories (N) during the period of 2010–2020. G' and S' denote the anthropogenic CH₄ flux from the in-situ and satellite inversion ensembles in the previous study (Deng et al., 2022) respectively, while G and S denote the fluxes from the in-situ and satellite inversion ensembles used in this study. N denotes the estimates from NGHGI. Grey, yellow, and brown bars represent the CH₄ fluxes from the sectors of fossil fuel combustion, agriculture and waste, and biomass burning respectively. On top of NGHGI emissions, emissions from ultra-emitters (red) are added to NGHGI estimates (diagnosed from S5P-TROPOMI measurements for the period 2019–2020; Lauvaux et al., 2022).

In our previous study, we found that satellite inversion models appear to have a better agreement with NGHGI than in-situ stations based inversion models, and on the other hand, that differences between inversion models and NGHGI in large oil- and gas-producing countries suggest an underestimation of national reports, possibly due to the omission of ultra-emitting sources by NGHGI. With the new inversion ensemble in this study, we confirm those results (Fig 10). In countries such as CHN, IND, and RUS, the updated inversion model set provides estimates that are closer to NGHGI, but differences still exist, and the reasons for these differences are not the same. For example, differences in anthropogenic methane emissions in IND are mainly due to differences in agricultural and waste methane flux with the new inversion ensemble used in this study. In RUS, the updated inversion ensemble shows lower fossil fuel emissions, reducing the difference with NGHGI for this sector, but higher agricultural and waste emissions than in Deng et al. (2022). Nevertheless, the updated fossil fuel emission flux is still higher than the NGHGI estimate for RUS. The remaining differences may be attributed to ultra-emitting sources or underestimated emission factors for some components of the oil and gas extraction and distribution industry in RUS. Conversely, in GULF, the new inversion model ensemble consistently reflects higher fossil fuel emission fluxes than NGHGI



like in our previous study, and expands the difference in estimates of artificial methane flux between inversion models and NGHGs, possibly indicating more methane leakage.

820 6.4 Influence of the prior used in CH₄ inversions

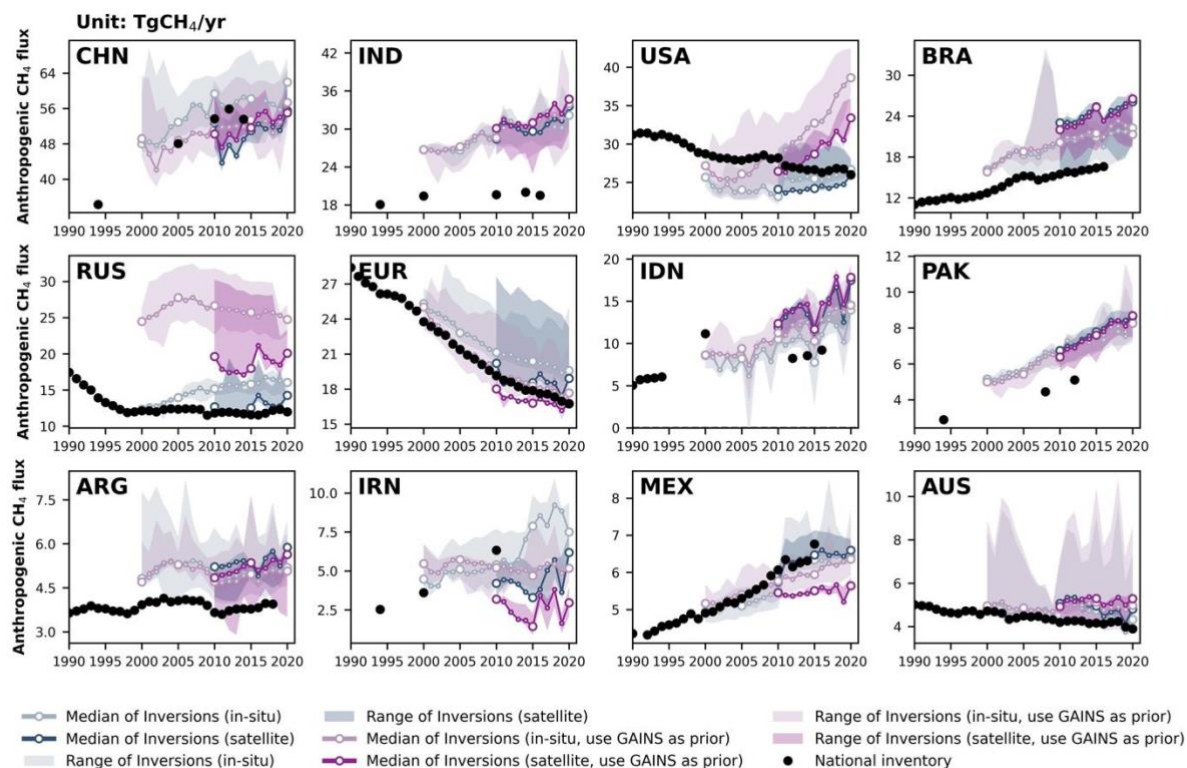


Figure 11. Total anthropogenic CH₄ fluxes for the 12 top emitters: China (CHN), India (IND), United States (USA), Brazil (BRA), Russia (RUS), European Union (EUR), Indonesia (IDN), Pakistan (PAK), Argentina (ARG), Iran (IRN), Mexico (MEX), and Australia (AUS).

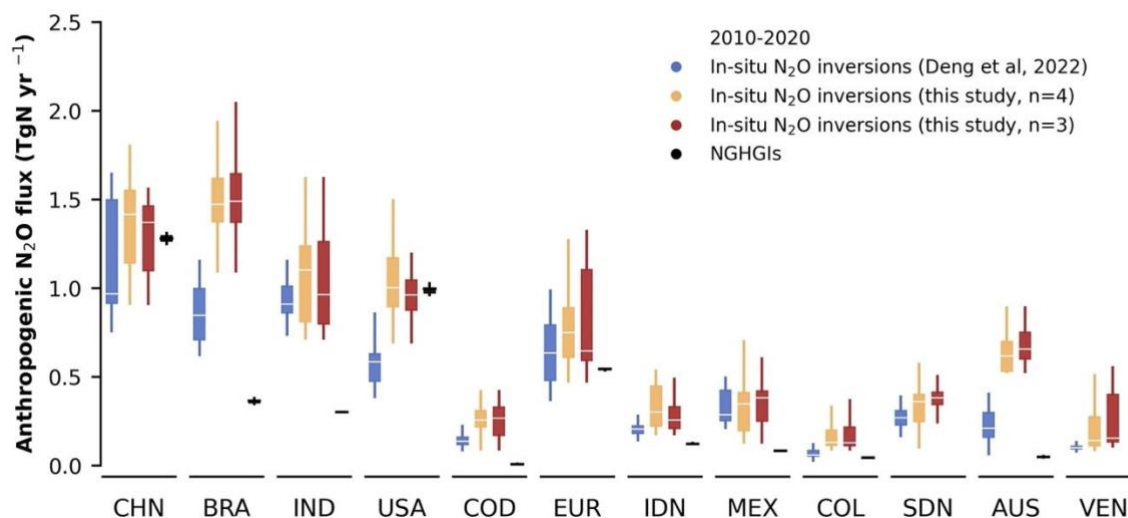
825 The black dots denote the reported values from NGHGs. The light blue lines/areas denote the median and maximum-minimum ranges of in-situ CH₄ inversions based on EDGARv6.0 as the prior and the dark blue ones of satellite inversions, respectively. The light purple lines/areas denote the median and maximum-minimum ranges of in-situ CH₄ inversions based on GAINS (Höglund-Isaksson et al., 2020) as the prior and the dark purple ones of satellite inversions, respectively.

The use of different priors can also influence the inversion results of the data. **Fig 11** presents the sets of inversion results using EDGAR (blue) and GAINS (purple) as priors. In most countries, the median values of the two inversion result sets are similar. However, in countries such as RUS, USA, IRN, MEX, significant differences are observed between the two inversion result sets, which may primarily stem from the differences in the inversion results for fossil CH₄ emissions (**SI Fig 2**). In RUS and USA, the inversion results using GAINS as priors are consistently higher than those using EDGAR as priors. In RUS, the satellite inversion results using GAINS as priors are higher by 45% during 2010-2020, and the ground-based inversion results are higher by 75% during 2000-2020. In the case of the USA, the inversion results using GAINS as priors exhibit a completely



835 different trend compared to the ones obtained using NGHGIs and EDGAR as priors. The inversion results using GAINS as
priors, both from satellite and ground-based measurements, show a rapid growth trend by increasing 24% from 2010 to 2020.
In IRN and MEX, the inversion results using GAINS as priors are lower than those using EDGAR as priors. For IRN, the
differences between satellite inversion results using different priors are not significant, and the trends are similar. However,
the ground-based inversion results are very close between 2000-2013, but after 2013, a steep increase is observed in the ground-
840 based inversion results using GAINS as priors. On the other hand, in MEX, the ground-based inversion results are similar, but
the satellite inversion results using GAINS as priors are relatively lower by 14% averagely.

6.5 Comparing anthropogenic N₂O flux with the previous study



845 **Figure 12.** Anthropogenic N₂O fluxes during the period of 2010-2020 in China (CHN), Brazil (BRA), India (IND), United States
(USA), Democratic Republic of the Congo (COD), European Union (EUR), Indonesia (IDN), Mexico (MEX), Colombia (COL), SDN
(Sudan), Australia (AUS), and Venezuela (VEN). Blue boxes denote the in-situ inversion results from Deng et al. 2022 processed from
Global Carbon Budget 2020 (Friedlingstein et al., 2020). Dark yellow boxes denote the inversion results processed in this study. Black boxes
denote the NGHGIs reported values.

Overall, the updated N₂O inversion results are systematically higher than the previous N₂O inversion results in most countries,
850 resulting in larger discrepancies between N₂O inversion results and NGHGIs (**Fig 12**). However, in the case of the USA, the
median of our N₂O inversion results is very close to NGHGIs. In addition, in countries such as IND, IDN, COL, CDN, and
VEN, our N₂O inversion results have a larger distribution compared to the previous study, indicating that the new N₂O
inversion ensemble (n=4) has less consistency in these countries compared to the previous ensemble (n=3).



Conclusions

855 This study reconciles the gap between atmospheric inversions and UNFCCC NGHGs for each of the three greenhouse gases, based on the post-processing framework we proposed in our previous study (Deng et al., 2022). We update inversion results and NGHGs datasets to present the most-up-to-date discrepancies between these two estimates. For CO₂, we updated the inversion results up to 2021, added a new inversion ensemble including inversions based on satellite observations, and applied a new mask of national managed land based on NGHGI reports in Russia, Brazil and Canada. For CH₄, we compared NGHGs and CH₄ inversion results up to 2020 by splitting the anthropogenic fluxes from inversions by aggregating prior estimates from 860 each sector or by removing fluxes of natural processes and discussed the uncertainties by using different priors in CH₄ inversions. For N₂O, we updated the inversion results up to 2019 and included the MIROC4-ACTM N₂O inversion, also separated the fluxes from managed land by using the same method on CO₂.

In the case of CO₂, In this study, we updated the managed land mask for Canada, Brazil, and Russia based on maps derived 865 from NGHGs and adjusted tree-cover thresholds. The analysis of different managed land mask definitions shows that the new mask, which is more consistent with the definition of managed land in the NGHGs for these countries, improves the agreement between managed land CO₂ fluxes and NGHGs in Russia and Canada. However, in Brazil, the new mask increases the gap between the estimated land carbon emissions and NGHGs. Further analysis is needed to understand the sources and reasons for discrepancies and uncertainties between inversion estimates and NGHGs. Thus, we still recommend that countries should 870 report their managed land in a spatially explicit manner to enable a better evaluation of national emission reports using inversions (and other observation-based approaches), and countries should also follow the recommendations of the IPCC 2006 Guidelines encouraging countries to use atmospheric data as an independent check on their national reports (IPCC 2006, 2019). Three additional satellite-based inversion results have been introduced for comparison with the in-situ inversion results and NGHGs. In some countries, the satellite-based inversions demonstrate better consistency with NGHGs compared to the in- 875 situ inversion models.

For CH₄, despite the large spread of inversions, both in-situ and GOSAT inversions show systematic differences with NGHGs. We also found that Kazakhstan and Turkmenistan in Central Asia and the Gulf countries in the Middle East, characterized by oil- and gas-producing industries, report much less CH₄ emissions than atmospheric inversions estimates. While in this region, there are few ground stations, and inversions depend on their prior fluxes, the fact that GOSAT and in-situ based inversions 880 point to NGHGI emissions being underestimated suggests areas for future research to constrain the emissions of these countries. We recommend here to develop regional campaigns (such as those performed in Alvarez et al. (2018)), to refine emission factors, and to track regional oil, gas and coal basins emissions and ultra-emitter site-level emissions using new tools (such as moderate and high-resolution satellite imagery).

For N₂O, the prevalence of large tropical natural sources, being outside the responsibility of countries if they are located on 885 unmanaged lands, has been overlooked before. For example, nearly half of the forests in Brazil are unmanaged according to its national inventory report. We did not solve this problem, but highlighted it and proposed a new method to remove natural



emissions from inversion total emissions. As many non-Annex I countries, which will have to produce inventories for the global stocktake are tropical countries with a very active nitrogen cycle and large natural N₂O emissions, a decoupling will exist between targeted emissions reductions and the observed growth rate of N₂O: it may hamper the eventual effectiveness of mitigation policies, that are directly reflected in the UNFCCC NGHGs reports, especially for this greenhouse gas. It is fair to say that the uncertainty from the spread of different inversions is large enough that inversions cannot ‘falsify’ N₂O NGHGs in most instances. Nevertheless, for CH₄ in countries around the Persian Gulf and Central Asia, and to some extent in Russia, and for N₂O in tropical countries, Mexico and Australia, we found that NGHGs emissions are significantly lower than inversions, which suggests that activity data or emission factors may need to be re-evaluated. Despite their large spread, inversions have the advantage of providing fluxes that are consistent with the accurately observed growth rates of each greenhouse gas in the atmosphere. The uncertainty of inversions is mainly a systematic bias due to internal settings or to the choice of a transport model. It does not mean that inversions cannot be used for monitoring interannual variability and trends of fluxes, in response to mitigation efforts, since most of their bias should have a small temporal component.

The study of global inversions at the country scale rather than at the traditional subcontinent scale (e.g. the “Transcom3 regions” of Gurney et al. (2002)) obviously pushes inversions close to the limit of their domain of validity, even in the case of large countries. The densification of observation networks and systems, especially from space, increases the observational information available at all spatial scales and gradually makes it possible to study smaller countries and reduce uncertainties of inversion results. This densification must be accompanied by a corresponding increase in the horizontal resolution of inversion systems (both the transport model and the control vector to be optimized). Note that the spatial resolution of most inverse models such as those contributing to the global carbon/methane/nitrous oxide budget is larger than 1 degree (see Table A4 in Friedlingstein et al. (2022), Table S6 in Saunio et al. (2020), and Table 1 in Tian et al. (2023)). They will likely soon have to go below one degree on a global scale to remain competitive for this type of study, despite the high computational challenge posed by the atmospheric inversion of long-lived tracers.

Data availability

Processed GHG (CO₂, CH₄, and N₂O) data from inverse models and UNFCCC NGHGs are available at <https://doi.org/10.5281/zenodo.10841716> (Deng et al., 2024).

This dataset contains 5 data files:

- The file *Inversions_CO2_v2022.csv* includes the NEE CO₂ flux from managed lands for the nine CO₂ inverse models. It includes 8 fields: years (from 1960 to 2021), country, value (unit: TgC/yr), sector (“land”: without the adjustment of lateral C flux; “land_cor”: with later C flux adjustment), source, gas, observation (“in-situ”: in-situ-based; “satellite”: satellite-based), version (“CO₂_ML_v2022” only).



- The file *Inversions_CH4_v2022.csv* includes CH₄ flux from anthropogenic sources for the six CH₄ inverse models. It includes 8 fields: years (from 2000 to 2020), country, value (unit: TgCH₄/yr), sector (“agrw”: agriculture and waste; “fos”: fossil fuel; ‘ant’: anthropogenic=agrw+fos), source, gas, observation (“in-situ”: in-situ-based; “satellite”: satellite-based), version (“CH₄_2022_V1”: use EDGAR as priors; “CH₄_2022_V2”: use GAINS as priors).
920
- The file *Inversions_N2O_v2022.csv* includes the anthropogenic N₂O flux from managed lands for the four N₂O inverse models. It includes 8 fields: years (from 1995 to 2020), country, value (unit: TgN₂O/yr), sector (“ant” only, for anthropogenic), source, gas, observation (“in-situ” only, for in-situ-based), version (“N₂O_ML_v2022” only).
- The file *lateral_CO2_v2022.csv* includes the national lateral C flux from river and trade.
- 925 - The file *NGHGs_v2022.csv* includes the national inventory data collected from UNFCCC NGHGs (unit: Gg/yr)

Author contribution

PC, FC, MS, RLT, and ZD designed and coordinated the study. PC, MS, RLT, and FC designed the framework of atmosphere inversion data processing. ZD, PC, LH, MS, RLT, and FC performed the post-processing and analysis and wrote the paper. ZD, LH, and TW compiled the national greenhouse gas inventories. MS, RLT, HT, and FC gathered the global atmosphere
930 inversion datasets of CO₂, CH₄, and N₂O. GG contributed the managed land mask of Brazil and Canada. FC processed the atmosphere inversion data with masks of managed lands and country boundaries. AT, SM, RJ, YN, BZ, JT, DB and AS contribute the unpublished CH₄ inversion data. All authors contributed to the full text.

Competing interests

At least one of the (co-)authors is a member of the editorial board of Earth System Science Data.

935 Acknowledgements

The authors are very grateful to the atmosphere inversion model developers Aki Tsuruta, Arjo Segers, Bo Zheng, Chris Wilson, Christian Rödenbeck, Kelley Wells, Liesbeth Florentie, Misa Ishizawa, Naveen Chandra, Peter Bergamaschi, Prabir Patra, Shamil Maksyutov, Yi Yin, and Yosuke Niwa for the availability of their global CO₂, CH₄, and N₂O inversion data and
940 acknowledge many other data providers (measurements, models, inventories, atmospheric inversions, hybrid products, etc.) that are directly or indirectly used in this synthesis.

References

Aragão, L. E. O. C., Anderson, L. O., Fonseca, M. G., Rosan, T. M., Vedovato, L. B., Wagner, F. H., Silva, C. V. J., Silva Junior, C. H. L., Arai, E., Aguiar, A. P., Barlow, J., Berenguer, E., Deeter, M. N., Domingues, L. G., Gatti, L., Gloor, M., Malhi, Y., Marengo, J. A.,



- 945 Miller, J. B., Phillips, O. L., and Saatchi, S.: 21st Century drought-related fires counteract the decline of Amazon deforestation carbon emissions, *Nat. Commun.*, 9, 536, 2018.
- Berchet, A., Sollum, E., Thompson, R. L., Pison, I., Thanwerdas, J., Broquet, G., Chevallier, F., Aalto, T., Berchet, A., Bergamaschi, P., Brunner, D., Engelen, R., Fortems-Cheiney, A., Gerbig, C., Groot Zwaafink, C. D., Haussaire, J.-M., Henne, S., Houweling, S., Karstens, U., Kutsch, W. L., Luijkx, I. T., Monteil, G., Palmer, P. I., van Peet, J. C. A., Peters, W., Peylin, P., Potier, E., Rödenbeck, C., Saunio, M., Scholze, M., Tsuruta, A., and Zhao, Y.: The Community Inversion Framework v1.0: a unified system for
950 atmospheric inversion studies, *Geoscientific Model Development*, 14, 5331–5354, 2021.
- Byrne, B., Liu, J., Lee, M., Yin, Y., Bowman, K. W., Miyazaki, K., Norton, A. J., Joiner, J., Pollard, D. F., Griffith, D. W. T., Velazco, V. A., N. M. Deutscher, Jones, N. B., and Paton-Walsh, C.: The carbon cycle of southeast Australia during 2019–2020: Drought, fires, and subsequent recovery, *AGU Advances*, 2, <https://doi.org/10.1029/2021av000469>, 2021.
- Byrne, B., Baker, D. F., Basu, S., Bertolacci, M., Bowman, K. W., Carroll, D., Chatterjee, A., Chevallier, F., Ciais, P., Cressie, N., Crisp,
955 D., Crowell, S., Deng, F., Deng, Z., Deutscher, Nicholas M., Dubey, M. K., Feng, S., García, O. E., Griffith, D. W. T., Herkommer, B., Hu, L., Jacobson, A. R., Janardanan, R., Jeong, S., Johnson, M. S., Jones, D. B. A., Kivi, R., Liu, J., Liu, Z., Maksyutov, S., Miller, J. B., Miller, S. M., Morino, I., Notholt, J., Oda, T., O'Dell, C. W., Oh, Y.-S., Ohyama, H., Patra, P. K., Peiro, H., Petri, C., Philip, S., Pollard, D. F., Poulter, B., Remaud, M., Schuh, A., Sha, M. K., Shiomi, K., Strong, K., Sweeney, C., Té, Y., Tian, H., Velazco, V. A., Vrekoussis, M., Warneke, T., Worden, J. R., Wunch, D., Yao, Y., Yun, J., Zammit-Mangion, A., and Zeng, N.:
960 National CO₂ budgets (2015–2020) inferred from atmospheric CO₂ observations in support of the global stocktake, *Earth System Science Data*, 15, 963–1004, 2023.
- Chandra, N., Patra, P. K., Bisht, J. S. H., Ito, A., Umezawa, T., Saigusa, N., Morimoto, S., Aoki, S., Janssens-Maenhout, G., Fujita, R., Takigawa, M., Watanabe, S., Saitoh, N., and Canadell, J. G.: Emissions from the Oil and Gas Sectors, Coal Mining and Ruminant Farming Drive Methane Growth over the Past Three Decades, *Journal of the Meteorological Society of Japan. Ser. II*, 99, 309–337,
965 2021.
- Chang, J., Ciais, P., Gasser, T., Smith, P., Herrero, M., Havlík, P., Obersteiner, M., Guenet, B., Goll, D. S., Li, W., Naipal, V., Peng, S., Qiu, C., Tian, H., Viovy, N., Yue, C., and Zhu, D.: Climate warming from managed grasslands cancels the cooling effect of carbon sinks in sparsely grazed and natural grasslands, *Nat. Commun.*, 12, 118, 2021.
- Chevallier, F.: Fluxes of carbon dioxide from managed ecosystems estimated by national inventories compared to atmospheric inverse
970 modeling, *Geophys. Res. Lett.*, 48, <https://doi.org/10.1029/2021gl093565>, 2021.
- Chevallier, F., Fisher, M., Peylin, P., Serrar, S., Bousquet, P., Bréon, F.-M., Chédin, A., and Ciais, P.: Inferring CO₂ sources and sinks



- from satellite observations: Method and application to TOVS data, *J. Geophys. Res.*, 110, <https://doi.org/10.1029/2005jd006390>, 2005.
- 975 Ciais, P., Yao, Y., Gasser, T., Baccini, A., Wang, Y., Lauerwald, R., Peng, S., Bastos, A., Li, W., Raymond, P. A., Canadell, J. G., Peters, G. P., Andres, R. J., Chang, J., Yue, C., Dolman, A. J., Haverd, V., Hartmann, J., Laruelle, G., Konings, A. G., King, A. W., Liu, Y., Luyssaert, S., Maignan, F., Patra, P. K., Peregon, A., Regnier, P., Pongratz, J., Poulter, B., Shvidenko, A., Valentini, R., Wang, R., Broquet, G., Yin, Y., Zscheischler, J., Guenet, B., Goll, D. S., Ballantyne, A.-P., Yang, H., Qiu, C., and Zhu, D.: Empirical estimates of regional carbon budgets imply reduced global soil heterotrophic respiration, *Natl Sci Rev*, 8, nwaal45, 2021.
- 980 Cui, X., Zhou, F., Ciais, P., Davidson, E. A., Tubiello, F. N., Niu, X., Ju, X., Canadell, J. G., Bouwman, A. F., Jackson, R. B., Mueller, N. D., Zheng, X., Kanter, D. R., Tian, H., Adalibieke, W., Bo, Y., Wang, Q., Zhan, X., and Zhu, D.: Global mapping of crop-specific emission factors highlights hotspots of nitrous oxide mitigation, *Nat Food*, 2, 886–893, 2021.
- Deng, Z., Ciais, P., Tzompa-Sosa, Z. A., Saunio, M., Qiu, C., Tan, C., Sun, T., Ke, P., Cui, Y., Tanaka, K., Lin, X., Thompson, R. L., Tian, H., Yao, Y., Huang, Y., Lauerwald, R., Jain, A. K., Xu, X., Bastos, A., Sitch, S., Palmer, P. I., Lauvaux, T., d’Aspremont, A., Giron, C., Benoit, A., Poulter, B., Chang, J., Petrescu, A. M. R., Davis, S. J., Liu, Z., Grassi, G., Albergel, C., Tubiello, F. N., 985 Perugini, L., Peters, W., and Chevallier, F.: Comparing national greenhouse gas budgets reported in UNFCCC inventories against atmospheric inversions, *Earth Syst. Sci. Data*, 14, 1639–1675, 2022.
- Deng, Z., Ciais, P., Hu, L., Wang, T., Martinez, A., Saunio, M., Thompson, R., and Chevallier, F.: Global greenhouse gas reconciliation 2022, 2024.
- Feng, L., Palmer, P. I., Parker, R. J., N. M. Deutscher, Feist, D. G., Kivi, R., Morino, I., and Sussmann, R.: Estimates of European uptake 990 of CO₂ inferred from GOSAT XCO₂ retrievals: sensitivity to measurement bias inside and outside Europe, *Atmos. Chem. Phys.*, 16, 1289–1302, 2016.
- Friedlingstein, P., O’Sullivan, M., Jones, M. W., Andrew, R. M., Hauck, J., Olsen, A., Peters, G. P., Peters, W., Pongratz, J., Sitch, S., Le Quéré, C., Canadell, J. G., Ciais, P., Jackson, R. B., Alin, S., Aragão, L. E. O. C., Arneeth, A., Arora, V., Bates, N. R., Becker, M., Benoit-Cattin, A., Bittig, H. C., Bopp, L., Bultan, S., Chandra, N., Chevallier, F., Chini, L. P., Evans, W., Florentie, L., Forster, P. 995 M., Gasser, T., Gehlen, M., Gilfillan, D., Gkritzalis, T., Gregor, L., Gruber, N., Harris, I., Hartung, K., Haverd, V., Houghton, R. A., Ilyina, T., Jain, A. K., Joetzjer, E., Kadono, K., Kato, E., Kitidis, V., Korsbakken, J. I., Landschützer, P., Lefèvre, N., Lenton, A., Lienert, S., Liu, Z., Lombardozzi, D., Marland, G., Metzl, N., Munro, D. R., Nabel, J. E. M. S., Nakaoka, S.-I., Niwa, Y., O’Brien, K., Ono, T., Palmer, P. I., Pierrot, D., Poulter, B., Resplandy, L., Robertson, E., Rödenbeck, C., Schwinger, J., Séférian, R., Skjelvan, I., Smith, A. J. P., Sutton, A. J., Tanhua, T., Tans, P. P., Tian, H., Tilbrook, B., van der Werf, G., Vuichard, N., Walker, A. P.,



- 1000 Wanninkhof, R., Watson, A. J., Willis, D., Wiltshire, A. J., Yuan, W., Yue, X., and Zaehle, S.: Global carbon budget 2020, *Earth Syst. Sci. Data*, 12, 3269–3340, 2020.
- Friedlingstein, P., O’Sullivan, M., Jones, M. W., Andrew, R. M., Gregor, L., Hauck, J., Le Quéré, C., Luijkx, I. T., Olsen, A., Peters, G. P., Peters, W., Pongratz, J., Schwingshackl, C., Sitch, S., Canadell, J. G., Ciais, P., Jackson, R. B., Alin, S. R., Alkama, R., Arneth, A., Arora, V. K., Bates, N. R., Becker, M., Bellouin, N., Bittig, H. C., Bopp, L., Chevallier, F., Chini, L. P., Cronin, M., Evans, W., Falk, S., Feely, R. A., Gasser, T., Gehlen, M., Gkritzalis, T., Gloege, L., Grassi, G., Gruber, N., Gürses, Ö., Harris, I., Hefner, M., Houghton, R. A., Hurtt, G. C., Iida, Y., Ilyina, T., Jain, A. K., Jersild, A., Kadono, K., Kato, E., Kennedy, D., Klein Goldewijk, K., Knauer, J., Korsbakken, J. I., Landschützer, P., Lefèvre, N., Lindsay, K., Liu, J., Liu, Z., Marland, G., Mayot, N., McGrath, M. J., Metzl, N., Monacchi, N. M., Munro, D. R., Nakaoka, S.-I., Niwa, Y., O’Brien, K., Ono, T., Palmer, P. I., Pan, N., Pierrot, D., Pöcöck, K., Poulter, B., Resplandy, L., Robertson, E., Rödenbeck, C., Rodriguez, C., Rosan, T. M., Schwinger, J., Séférian, R., Shutler, J. D., Skjelvan, I., Steinhoff, T., Sun, Q., Sutton, A. J., Sweeney, C., Takao, S., Tanhua, T., Tans, P. P., Tian, X., Tian, H., Tilbrook, B., Tsujino, H., Tubiello, F., van der Werf, G. R., Walker, A. P., Wanninkhof, R., Whitehead, C., Willstrand Wranne, A., et al.: Global Carbon Budget 2022, *Earth System Science Data*, 14, 4811–4900, 2022.
- 1010 Gatti, L. V., Basso, L. S., Miller, J. B., Gloor, M., Gatti Domingues, L., Cassol, H. L. G., Tejada, G., Aragão, L. E. O. C., Nobre, C., Peters, W., Marani, L., Arai, E., Sanches, A. H., Corrêa, S. M., Anderson, L., Von Randow, C., Correia, C. S. C., Crispim, S. P., and Neves, R. A. L.: Amazonia as a carbon source linked to deforestation and climate change, *Nature*, 595, 388–393, 2021.
- 1015 Gatti, L. V., Cunha, C. L., Marani, L., Cassol, H. L. G., Messias, C. G., Arai, E., Denning, A. S., Soler, L. S., Almeida, C., Setzer, A., Domingues, L. G., Basso, L. S., Miller, J. B., Gloor, M., Correia, C. S. C., Tejada, G., Neves, R. A. L., Rajao, R., Nunes, F., Filho, B. S. S., Schmitt, J., Nobre, C., Corrêa, S. M., Sanches, A. H., Aragão, L. E. O. C., Anderson, L., Von Randow, C., Crispim, S. P., Silva, F. M., and Machado, G. B. M.: Increased Amazon carbon emissions mainly from decline in law enforcement, *Nature*, 621, 318–323, 2023.
- 1020 Grassi, G., Stehfest, E., Rogelj, J., van Vuuren, D., Cescatti, A., House, J., Nabuurs, G.-J., Rossi, S., Alkama, R., Viñas, R. A., Calvin, K., Ceccherini, G., Federici, S., Fujimori, S., Gusti, M., Hasegawa, T., Havlik, P., Humpenöder, F., Korosuo, A., Perugini, L., Tubiello, F. N., and Popp, A.: Critical adjustment of land mitigation pathways for assessing countries’ climate progress, *Nat. Clim. Chang.*, 11, 425–434, 2021.
- 1025 Grassi, G., Schwingshackl, C., Gasser, T., Houghton, R. A., Sitch, S., Canadell, J. G., Cescatti, A., Ciais, P., Federici, S., Friedlingstein, P., Kurz, W. A., Sanz Sanchez, M. J., Abad Viñas, R., Alkama, R., Bultan, S., Ceccherini, G., Falk, S., Kato, E., Kennedy, D., Knauer, J., Korosuo, A., Melo, J., McGrath, M. J., Nabel, J. E. M. S., Poulter, B., Romanovskaya, A. A., Rossi, S., Tian, H., Walker, A. P.,



- Yuan, W., Yue, X., and Pongratz, J.: Harmonising the land-use flux estimates of global models and national inventories for 2000–2020, *Earth System Science Data*, 15, 1093–1114, 2023.
- 1030 Hartmann, J., Jansen, N., Dürr, H. H., Kempe, S., and Köhler, P.: Global CO₂-consumption by chemical weathering: What is the contribution of highly active weathering regions?, *Glob. Planet. Change*, 69, 185–194, 2009.
- Höglund-Isaksson, L., Gómez-Sanabria, A., Klimont, Z., Rafaj, P., and Schöpp, W.: Technical potentials and costs for reducing global anthropogenic methane emissions in the 2050 timeframe –results from the GAINS model, *Environ. Res. Commun.*, 2, 025004, 2020.
- IPCC: Revised 1996 IPCC Guidelines for National Greenhouse Inventories, IPCC/OECD/IEA, Paris, France, 1997.
- 1035 IPCC: 2006 IPCC guidelines for National Greenhouse Gas Inventories, IGES, 2006.
- IPCC: 2019 Refinement to the 2006 IPCC Guidelines for National Greenhouse Gas Inventories, edited by: Buendia, E., Tanabe, K., Kranjc, A., Baasansuren, J., Fukuda, M., Ngarize, S., Osako, A., Pyrozhenko, Y., Shermanau, P., and Federici, S., Intergovernmental Panel on Climate Change (IPCC), Switzerland, 2019.
- IPCC: Climate Change 2023: Synthesis Report, IPCC, Geneva, Switzerland, 2023.
- 1040 Janssens-Maenhout, G., Crippa, M., Guizzardi, D., Muntean, M., Schaaf, E., Dentener, F., Bergamaschi, P., Pagliari, V., Olivier, J. G. J., Peters, J. A. H. W., van Aardenne, J. A., Monni, S., Doering, U., Petrescu, A. M. R., Solazzo, E., and Oreggioni, G. D.: EDGAR v4.3.2 Global Atlas of the three major greenhouse gas emissions for the period 1970–2012, *Earth Syst. Sci. Data*, 11, 959–1002, 2019.
- Jin, Z., Wang, T., Zhang, H., Wang, Y., Ding, J., and Tian, X.: Constraint of satellite CO₂ retrieval on the global carbon cycle from a Chinese atmospheric inversion system, *Sci. China Earth Sci.*, 66, 609–618, 2023.
- 1045 Jones, M. W., Andrew, R. M., Peters, G. P., Janssens-Maenhout, G., De-Gol, A. J., Dou, X., Liu, Z., Pickers, P., Ciais, P., Patra, P. K., Chevallier, F., and Le Quéré, C.: Gridded fossil CO₂ emissions and related O₂ combustion consistent with national inventories, 2022.
- Kaminski, T., Rayner, P. J., Heimann, M., and Enting, I. G.: On aggregation errors in atmospheric transport inversions, *J. Geophys. Res.* D: Atmos., 106, 4703–4715, 2001.
- 1050 Klein Goldewijk, K., Beusen, A., Doelman, J., and Stehfest, E.: Anthropogenic land use estimates for the Holocene – HYDE 3.2, *Earth Syst. Sci. Data*, 9, 927–953, 2017.
- Kong, Y., Zheng, B., Zhang, Q., and He, K.: Global and regional carbon budget for 2015–2020 inferred from OCO-2 based on an ensemble Kalman filter coupled with GEOS-Chem, *Atmos. Chem. Phys.*, 22, 10769–10788, 2022.
- 1055 van der Laan-Luijkx, I. T., van der Velde, I. R., van der Veen, E., Tsuruta, A., Stanislawska, K., Babenhauserheide, A., Zhang, H. F., Liu,



- Y., He, W., Chen, H., Masarie, K. A., Krol, M. C., and Peters, W.: The CarbonTracker Data Assimilation Shell (CTDAS) v1.0: implementation and global carbon balance 2001–2015, *Geosci. Model Dev.*, 10, 2785–2800, 2017.
- Lauvaux, T., Giron, C., Mazzolini, M., d’Aspremont, A., Duren, R., Cusworth, D., Shindell, D., and Ciais, P.: Global assessment of oil and gas methane ultra-emitters, *Science*, 375, 557–561, 2022.
- 1060 Liu, J., Baskaran, L., Bowman, K., Schimel, D., Bloom, A. A., Parazoo, N. C., Oda, T., Carroll, D., Menemenlis, D., Joiner, J., Commane, R., Daube, B., Gatti, L. V., McKain, K., Miller, J., Stephens, B. B., Sweeney, C., and Wofsy, S.: Carbon Monitoring System Flux Net Biosphere Exchange 2020 (CMS-Flux NBE 2020), *Earth System Science Data*, 13, 299–330, 2021.
- Maksyutov, S., Oda, T., Saito, M., Janardanan, R., Belikov, D., Kaiser, J. W., Zhuravlev, R., Ganshin, A., Valsala, V. K., Andrews, A., Chmura, L., Dlugokencky, E., Haszpra, L., Langenfelds, R. L., Machida, T., Nakazawa, T., Ramonet, M., Sweeney, C., and Worthy, 1065 D.: Technical note: A high-resolution inverse modelling technique for estimating surface CO₂ fluxes based on the NIES-TM–FLEXPART coupled transport model and its adjoint, *Atmos. Chem. Phys.*, 21, 1245–1266, 2021.
- Mason Earles, J., Yeh, S., and Skog, K. E.: Timing of carbon emissions from global forest clearance, *Nat. Clim. Chang.*, 2, 682–685, 2012.
- Mayorga, E., Seitzinger, S. P., Harrison, J. A., Dumont, E., Beusen, A. H. W., Bouwman, A. F., Fekete, B. M., Kroeze, C., and Van Drecht, G.: Global Nutrient Export from WaterSheds 2 (NEWS 2): Model development and implementation, *Environmental Modelling & Software*, 25, 837–853, 2010. 1070
- Naus, S., Domingues, L. G., Krol, M., Luijkx, I. T., Gatti, L. V., Miller, J. B., Gloor, E., Basu, S., Correia, C., Koren, G., Worden, H. M., Flemming, J., Pétron, G., and Peters, W.: Sixteen years of MOPITT satellite data strongly constrain Amazon CO fire emissions, *Atmos. Chem. Phys.*, 22, 14735–14750, 2022.
- Niwa, Y., Ishijima, K., Ito, A., and Iida, Y.: Toward a long-term atmospheric CO₂ inversion for elucidating natural carbon fluxes: technical notes of NISMON-CO₂ v2021.1, *Progress in Earth and Planetary Science*, 9, 1–19, 2022. 1075
- Ogle, S. M., Domke, G., Kurz, W. A., Rocha, M. T., Huffman, T., Swan, A., Smith, J. E., Woodall, C., and Krug, T.: Delineating managed land for reporting national greenhouse gas emissions and removals to the United Nations framework convention on climate change, *Carbon Balance Manag.*, 13, 9, 2018.
- Patra, P. K., Takigawa, M., Watanabe, S., Chandra, N., Ishijima, K., and Yamashita, Y.: Improved Chemical Tracer Simulation by 1080 MIROC4.0-based Atmospheric Chemistry-Transport Model (MIROC4-ACTM), *SOLAIAT*, 14, 91–96, 2018.
- Patra, P. K., Dlugokencky, E. J., Elkins, J. W., Dutton, G. S., Tohjima, Y., Sasakawa, M., Ito, A., Weiss, R. F., Manizza, M., Krummel, P. B., Prinn, R. G., O’doherly, S., Bianchi, D., Nevison, C., Solazzo, E., Lee, H., Joo, S., Kort, E. A., Maity, S., and Takigawa, M.: Forward and Inverse Modelling of Atmospheric Nitrous Oxide Using MIROC4-Atmospheric Chemistry-Transport Model, *Journal of*



the Meteorological Society of Japan. Ser. II, 100, 361–386, 2022.

- 1085 Peng, S., Lin, X., Thompson, R. L., Xi, Y., Liu, G., Hauglustaine, D., Lan, X., Poulter, B., Ramonet, M., Saunois, M., Yin, Y., Zhang, Z., Zheng, B., and Ciais, P.: Wetland emission and atmospheric sink changes explain methane growth in 2020, *Nature*, 612, 477–482, 2022.
- Perugini, L., Pellis, G., Grassi, G., Ciais, P., Dolman, H., House, J. I., Peters, G. P., Smith, P., Günther, D., and Peylin, P.: Emerging reporting and verification needs under the Paris Agreement: How can the research community effectively contribute?, *Environ. Sci. Policy*, 122, 116–126, 2021.
- 1090 Petrescu, A. M. R., McGrath, M. J., Andrew, R. M., Peylin, P., Peters, G. P., Ciais, P., Broquet, G., Tubiello, F. N., Gerbig, C., Pongratz, J., Janssens-Maenhout, G., Grassi, G., Nabuurs, G.-J., Regnier, P., Lauerwald, R., Kuhnert, M., Balkovič, J., Schelhaas, M.-J., Denier van der Gon, H. A. C., Solazzo, E., Qiu, C., Pilli, R., Konovalov, I. B., Houghton, R. A., Günther, D., Perugini, L., Crippa, M., Ganzenmüller, R., Luijkx, I. T., Smith, P., Munassar, S., Thompson, R. L., Conchedda, G., Monteil, G., Scholze, M., Karstens, U., Brockmann, P., and Dolman, A. J.: The consolidated European synthesis of CO₂ emissions and removals for the European Union and United Kingdom: 1990–2018, *Earth Syst. Sci. Data*, 13, 2363–2406, 2021.
- Philibert, A., Loyce, C., and Makowski, D.: Prediction of N₂O emission from local information with Random Forest, *Environ. Pollut.*, 177, 156–163, 2013.
- Potapov, P., Hansen, M. C., Laestadius, L., Turubanova, S., Yaroshenko, A., Thies, C., Smith, W., Zhuravleva, I., Komarova, A., Minnemeyer, S., and Esipova, E.: The last frontiers of wilderness: Tracking loss of intact forest landscapes from 2000 to 2013, *Sci Adv*, 3, e1600821, 2017.
- 1100 Regnier, P., Friedlingstein, P., Ciais, P., Mackenzie, F. T., Gruber, N., Janssens, I. A., Laruelle, G. G., Lauerwald, R., Luyssaert, S., Andersson, A. J., Arndt, S., Arnosti, C., Borges, A. V., Dale, A. W., Gallego-Sala, A., Goddérís, Y., Goossens, N., Hartmann, J., Heinze, C., Ilyina, T., Joos, F., LaRowe, D. E., Leifeld, J., Meysman, F. J. R., Munhoven, G., Raymond, P. A., Spahni, R., Suntharalingam, P., and Thullner, M.: Anthropogenic perturbation of the carbon fluxes from land to ocean, *Nat. Geosci.*, 6, 597–607, 2013.
- Rödenbeck, C., Houweling, S., Gloor, M., and Heimann, M.: CO₂ flux history 1982–2001 inferred from atmospheric data using a global inversion of atmospheric transport, *Atmos. Chem. Phys.*, 3, 1919–1964, 2003.
- Saunois, M., Stavert, A. R., Poulter, B., Bousquet, P., Canadell, J. G., Jackson, R. B., Raymond, P. A., Dlugokencky, E. J., Houweling, S., Patra, P. K., Ciais, P., Arora, V. K., Bastviken, D., Bergamaschi, P., Blake, D. R., Brailsford, G., Bruhwiler, L., Carlson, K. M., Carrol, M., Castaldi, S., Chandra, N., Crevoisier, C., Crill, P. M., Covey, K., Curry, C. L., Etiope, G., Frankenberg, C., Gedney, N.,



- Hegglin, M. I., Höglund-Isaksson, L., Hugelius, G., Ishizawa, M., Ito, A., Janssens-Maenhout, G., Jensen, K. M., Joos, F., Kleinen, T., Krummel, P. B., Langenfelds, R. L., Laruelle, G. G., Liu, L., Machida, T., Maksyutov, S., McDonald, K. C., McNorton, J., Miller, P. A., Melton, J. R., Morino, I., Müller, J., Murguia-Flores, F., Naik, V., Niwa, Y., Noce, S., O'Doherty, S., Parker, R. J., Peng, C., Peng, S., Peters, G. P., Prigent, C., Prinn, R., Ramonet, M., Regnier, P., Riley, W. J., Rosentreter, J. A., Segers, A., Simpson, I. J., Shi, H., Smith, S. J., Steele, L. P., Thornton, B. F., Tian, H., Tohjima, Y., Tubiello, F. N., Tsuruta, A., Viovy, N., Voulgarakis, A., Weber, T. S., van Weele, M., van der Werf, G. R., Weiss, R. F., Worthy, D., Wunch, D., Yin, Y., Yoshida, Y., Zhang, W., Zhang, Z., Zhao, Y., Zheng, B., Zhu, Q., Zhu, Q., and Zhuang, Q.: The global methane budget 2000–2017, *Earth Syst. Sci. Data*, 12, 1561–1623, 2020.
- 1115
- Schuldt, K. N., Mund, J., Lujikx, I. T., Aalto, T., Abshire, J. B., Aikin, K., Andrews, A., Aoki, S., Apadula, F., Baier, B., Bakwin, P., Bartyzel, J., Bentz, G., Bergamaschi, P., Beyersdorf, A., Biermann, T., Biraud, S. C., Boenisch, H., Bowling, D., Brailsford, G., van den Bulk, P., Chen, G., Chen, H., Chmura, L., Clark, S., Climadat, S., Della Coletta, J., Colomb, A., Commane, R., Conil, S., Cox, A., Cristofanelli, P., Cuevas, E., Curcoll, R., Daube, B., Davis, K., Delmotte, M., DiGangi, J. P., van Dinter, D., Dlugokencky, E., Elkins, J. W., Emmenegger, L., Fang, S., Fischer, M. L., Forster, G., Frumau, A., Galkowski, M., Gatti, L. V., Gehrlein, T., Gerbig, C., Gheusi, F., Gloor, E., Gomez-Trueba, V., Goto, D., Griffis, T., Hammer, S., Hanson, C., Haszpra, L., Hatakka, J., Heimann, M., Heliasz, M., Hensen, A., Hermanssen, O., Hints, E., Holst, J., Ivakhov, V., Jaffe, D., Joubert, W., Karion, A., Kawa, S. R., Kazan, V., Keeling, R., Keronen, P., Kolari, P., Kominkova, K., Kort, E., Kozlova, E., Krummel, P., Kubistin, D., Labuschagne, C., Lam, D. H. Y., Langenfelds, R., Laurent, O., Laurila, T., Lauvaux, T., Lavric, J., Law, B., Lee, J., Lee, O. S. M., Lehner, I., Leppert, R., Leuenberger, M., Levin, I., Levula, J., Lin, J., Lindauer, M., Loh, Z., Lopez, M., Machida, T., et al.: Multi-laboratory compilation of atmospheric carbon dioxide data for the period 1957–2020; obspack_co2_1_GLOBALVIEWplus_v7.0_2021-08-18, 2021.
- 1120
- Schuldt, K. N., Jacobson, A. R., Aalto, T., Andrews, A., Bakwin, P., Bergamaschi, P., Biermann, T., Biraud, S. C., Chen, H., Colomb, A., Conil, S., Cristofanelli, P., Delmotte, M., Dlugokencky, E., Emmenegger, L., Fischer, M. L., Hatakka, J., Heliasz, M., Hermanssen, O., Holst, J., Jaffe, D., Karion, A., Kazan, V., Keronen, P., Kominkova, K., Kubistin, D., Laurent, O., Laurila, T., Lee, J., Lehner, I., Leuenberger, M., Lindauer, M., Lopez, M., Mammarella, I., Manca, G., Marek, M. V., De Mazière, M., McKain, K., Miller, C. E., Miller, J. B., Mölder, M., Müller-Williams, J., Myhre, C. L., Piacentino, S., Pichon, J. M., Plass-Duelmer, C., Plass-Duelmer, C., Ramonet, M., di Sarra, A. G., Scheeren, B., Schumacher, M., Sha, M. K., Sloop, C. D., Smith, P., Steinbacher, M., Sweeney, C., Tans, P., Thoning, K., Tørseth, K., Trisolino, P., Viner, B., Vitkova, G., and De Wekker, S.: Multi-laboratory compilation of atmospheric carbon dioxide data for the year 2022; obspack_co2_1_NRT_v7.2_2022-06-28, 2022.
- 1125
- Segers, A. and Houweling, S.: Description of the CH₄ Inversion Production Chain, Copernicus Atmosphere Monitoring Service, 2017.
- 1130
- 1135



- 1140 Shcherbak, I., Millar, N., and Robertson, G. P.: Global metaanalysis of the nonlinear response of soil nitrous oxide (N₂O) emissions to fertilizer nitrogen, *Proc. Natl. Acad. Sci. U. S. A.*, 111, 9199–9204, 2014.
- Thompson, R. L., Chevallier, F., Crotwell, A. M., Dutton, G., Langenfelds, R. L., Prinn, R. G., Weiss, R. F., Tohjima, Y., Nakazawa, T., Krummel, P. B., Steele, L. P., Fraser, P., O’Doherty, S., Ishijima, K., and Aoki, S.: Nitrous oxide emissions 1999 to 2009 from a global atmospheric inversion, *Atmos. Chem. Phys.*, 14, 1801–1817, 2014.
- 1145 Tian, H., Yang, J., Xu, R., Lu, C., Canadell, J. G., Davidson, E. A., Jackson, R. B., Arneeth, A., Chang, J., Ciais, P., Gerber, S., Ito, A., Joos, F., Lienert, S., Messina, P., Olin, S., Pan, S., Peng, C., Saikawa, E., Thompson, R. L., Vuichard, N., Winiwarter, W., Zaehle, S., and Zhang, B.: Global soil nitrous oxide emissions since the preindustrial era estimated by an ensemble of terrestrial biosphere models: Magnitude, attribution, and uncertainty, *Glob. Chang. Biol.*, 25, 640–659, 2019.
- Tian, H., Xu, R., Canadell, J. G., Thompson, R. L., Winiwarter, W., Suntharalingam, P., Davidson, E. A., Ciais, P., Jackson, R. B., 1150 Janssens-Maenhout, G., Prather, M. J., Regnier, P., Pan, N., Pan, S., Peters, G. P., Shi, H., Tubiello, F. N., Zaehle, S., Zhou, F., Arneeth, A., Battaglia, G., Berthet, S., Bopp, L., Bouwman, A. F., Buitenhuis, E. T., Chang, J., Chipperfield, M. P., Dangal, S. R. S., Dlugokencky, E., Elkins, J. W., Eyre, B. D., Fu, B., Hall, B., Ito, A., Joos, F., Krummel, P. B., Landolfi, A., Laruelle, G. G., Lauerwald, R., Li, W., Lienert, S., Maavara, T., MacLeod, M., Millet, D. B., Olin, S., Patra, P. K., Prinn, R. G., Raymond, P. A., Ruiz, D. J., van der Werf, G. R., Vuichard, N., Wang, J., Weiss, R. F., Wells, K. C., Wilson, C., Yang, J., and Yao, Y.: A 1155 comprehensive quantification of global nitrous oxide sources and sinks, *Nature*, 586, 248–256, 2020.
- Tian, H., Pan, N., Thompson, R. L., Canadell, J. G., Suntharalingam, P., Regnier, P., Davidson, E. A., Prather, M., Ciais, P., Muntean, M., Pan, S., Winiwarter, W., Zaehle, S., Zhou, F., Jackson, R. B., Bange, H. W., Berthet, S., Bian, Z., Bianchi, D., Bouwman, A. F., Buitenhuis, E. T., Dutton, G., Hu, M., Ito, A., Jain, A. K., Jeltsch-Thömmes, A., Joos, F., Kou-Giesbrecht, S., Krummel, P. B., Lan, X., Landolfi, A., Lauerwald, R., Li, Y., Lu, C., Maavara, T., Manizza, M., Millet, D. B., Mühle, J., Patra, P. K., Peters, G. P., Qin, X., 1160 Raymond, P., Resplandy, L., Rosentreter, J. A., Shi, H., Sun, Q., Tonina, D., Tubiello, F. N., van der Werf, G. R., Vuichard, N., Wang, J., Wells, K. C., Western, L. M., Wilson, C., Yang, J., Yao, Y., You, Y., and Zhu, Q.: Global Nitrous Oxide Budget 1980–2020, *Earth System Science Data Discussions*, 1–98, 2023.
- Tibrewal, K., Ciais, P., Saunio, M., Martinez, A., Lin, X., Thanwerdas, J., Deng, Z., Chevallier, F., Giron, C., Albergel, C., Tanaka, K., Patra, P., Tsuruta, A., Zheng, B., Belikov, D., Niwa, Y., Janardanan, R., Maksyutov, S., Segers, A., Tzompa-Sosa, Z. A., Bousquet, P., and Sciare, J.: Assessment of methane emissions from oil, gas and coal sectors across inventories and atmospheric inversions, 1165 *Commun. Earth Environ.*, 5, <https://doi.org/10.1038/s43247-023-01190-w>, 2024.
- Tsuruta, A., Aalto, T., Backman, L., Hakkarainen, J., van der Laan-Luijkx, I. T., Krol, M. C., Spahni, R., Houweling, S., Laine, M.,



- 1170 Dlugokencky, E., Gomez-Pelaez, A. J., van der Schoot, M., Langenfelds, R., Ellul, R., Arduini, J., Apadula, F., Gerbig, C., Feist, D., G., Kivi, R., Yoshida, Y., and Peters, W.: Global methane emission estimates for 2000–2012 from CarbonTracker Europe-CH4 v1.0, *Geosci. Model Dev.*, 10, 1261–1289, 2017.
- UNFCCC: Biennial Update Report submissions from Non-Annex I Parties, available at: <https://unfccc.int/BURs>, last access: 2 July 2021a.
- UNFCCC: National Communication submissions from Non-Annex I Parties, available at: <https://unfccc.int/non-annex-I-NCs>, last access: 5 December 2021b.
- 1175 Wang, F., Maksyutov, S., Tsuruta, A., Janardanan, R., Ito, A., Sasakawa, M., Machida, T., Morino, I., Yoshida, Y., Kaiser, J. W., Janssens-Maenhout, G., Dlugokencky, E. J., Mammarella, I., Lavric, J. V., and Matsunaga, T.: Methane Emission Estimates by the Global High-Resolution Inverse Model Using National Inventories, *Remote Sensing*, 11, 2489, 2019.
- Wang, J. A., Baccini, A., Farina, M., Randerson, J. T., and Friedl, M. A.: Disturbance suppresses the aboveground carbon sink in North American boreal forests, *Nat. Clim. Chang.*, 11, 435–441, 2021.
- 1180 Wang, Q., Zhou, F., Shang, Z., Ciais, P., Winiwarter, W., Jackson, R. B., Tubiello, F. N., Janssens-Maenhout, G., Tian, H., Cui, X., Canadell, J. G., Piao, S., and Tao, S.: Data-driven estimates of global nitrous oxide emissions from croplands, *Natl Sci Rev*, 7, 441–452, 2020.
- van Wees, D., van der Werf, G. R., Randerson, J. T., Rogers, B. M., Chen, Y., Veraverbeke, S., Giglio, L., and Morton, D. C.: Global biomass burning fuel consumption and emissions at 500 m spatial resolution based on the Global Fire Emissions Database (GFED), *Geoscientific Model Development*, 15, 8411–8437, 2022.
- 1185 Wells, K. C., Millet, D. B., Bousserrez, N., Henze, D. K., Chaliyakunnel, S., Griffis, T. J., Luan, Y., Dlugokencky, E. J., Prinn, R. G., O’Doherty, S., Weiss, R. F., Dutton, G. S., Elkins, J. W., Krummel, P. B., Langenfelds, R., Steele, L. P., Kort, E. A., Wofsy, S. C., and Umezawa, T.: Simulation of atmospheric N₂O with GEOS-Chem and its adjoint: evaluation of observational constraints, *Geosci. Model Dev.*, 8, 3179–3198, 2015.
- Wilson, C., Chipperfield, M. P., Gloor, M., and Chevallier, F.: Development of a variational flux inversion system (INVICAT v1.0) using the TOMCAT chemical transport model, *Geosci. Model Dev.*, 7, 2485–2500, 2014.
- 1190 Winkler, K., Yang, H., Ganzenmüller, R., Fuchs, R., Ceccherini, G., Duveiller, G., Grassi, G., Pongratz, J., Bastos, A., Shvidenko, A., Araza, A., Herold, M., Wigneron, J.-P., and Ciais, P.: Changes in land use and management led to a decline in Eastern Europe’s terrestrial carbon sink, *Communications Earth & Environment*, 4, 1–14, 2023.
- 1195 Xu, X., Sharma, P., Shu, S., Lin, T.-S., Ciais, P., Tubiello, F. N., Smith, P., Campbell, N., and Jain, A. K.: Global Greenhouse Gas Emissions from Plant-and Animal-Based Food, *Nature Food*, 2021.



- Yao, Y., Tian, H., Shi, H., Pan, S., Xu, R., Pan, N., and Canadell, J. G.: Increased global nitrous oxide emissions from streams and rivers in the Anthropocene, *Nat. Clim. Chang.*, 10, 138–142, 2019.
- Yin, Y., Chevallier, F., Ciais, P., Broquet, G., Fortems-Cheiney, A., Pison, I., and Saunois, M.: Decadal trends in global CO emissions as seen by MOPITT, *Atmos. Chem. Phys.*, 15, 13433–13451, 2015.
- 1200 Zheng, B., Chevallier, F., Ciais, P., Yin, Y., Deeter, M. N., Worden, H. M., Wang, Y., Zhang, Q., and He, K.: Rapid decline in carbon monoxide emissions and export from East Asia between years 2005 and 2016, *Environ. Res. Lett.*, 13, 044007, 2018.
- Zhou, F., Shang, Z., Zeng, Z., Piao, S., Ciais, P., Raymond, P. A., Wang, X., Wang, R., Chen, M., Yang, C., Tao, S., Zhao, Y., Meng, Q., Gao, S., and Mao, Q.: New model for capturing the variations of fertilizer-induced emission factors of N₂O, *Global Biogeochem. Cycles*, 29, 885–897, 2015.
- 1205 Zscheischler, J., Mahecha, M. D., Avitabile, V., Calle, L., Carvalhais, N., Ciais, P., Gans, F., Gruber, N., Hartmann, J., Herold, M., Ichii, K., Jung, M., Landschützer, P., Laruelle, G. G., Lauerwald, R., Papale, D., Peylin, P., Poulter, B., Ray, D., Regnier, P., Rödenbeck, C., Roman-Cuesta, R. M., Schwalm, C., Tramontana, G., Tyukavina, A., Valentini, R., van der Werf, G., West, T. O., Wolf, J. E., and Reichstein, M.: Reviews and syntheses: An empirical spatiotemporal description of the global surface–atmosphere carbon fluxes: opportunities and data limitations, *Biogeosciences*, 14, 3685–3703, 2017.